Differential Beamforming

J. Benesty, I. Cohen, and J. Chen,
Fundamentals of Signal Enhancement and Array Signal Processing,
Wiley-IEEE Press, 2017.

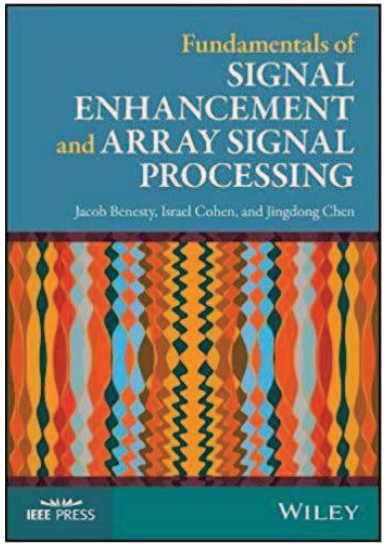

Outline

Introduction

Differential beamforming is a particular fixed beamforming.

Differential beamformers present two great features:

1. Frequency invariance, which is extremely important when dealing with broadband signals.
2. Highest gains in diffuse noise.

However, the main drawback is white noise amplification.

In this talk, we derive and study differential beamformers of different orders.

We explain the advantages as well as the main problem of this method, and show how to deal with the white noise amplification problem.

Signal Model and Problem Formulation

We consider a plane wave, in the farfield that propagates in an anechoic acoustic environment at the speed of sound, i.e., $c = 340$ m/s, and impinges on a uniform linear sensor array consisting of M omnidirectional microphones (see Fig. 1).

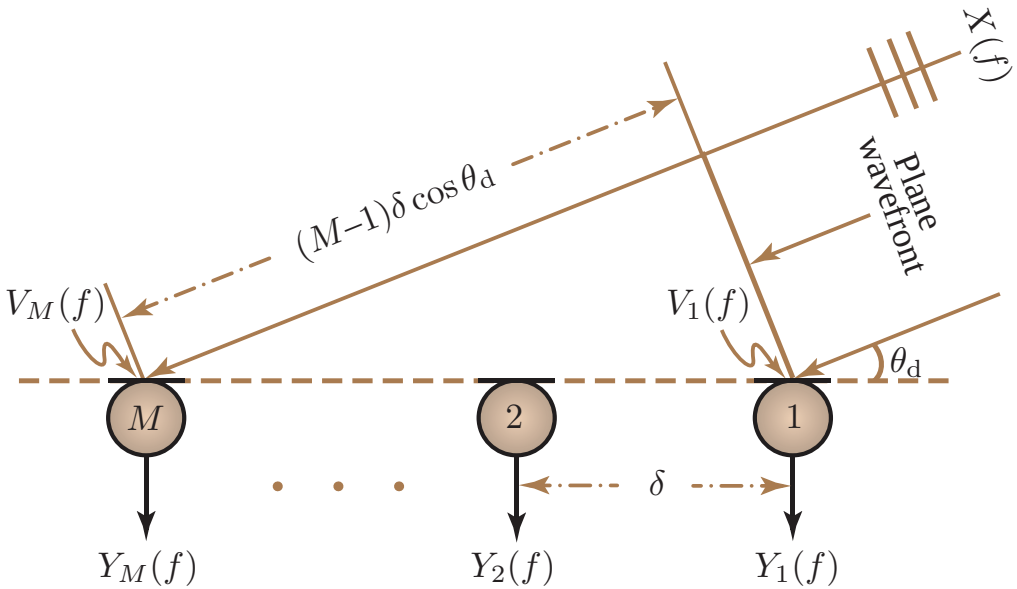

Figure 1: A uniform linear array with M sensors.

The observation vector is then [1]

$$\begin{aligned}\mathbf{y}(f) &= \left[\begin{array}{cccc} Y_1(f) & Y_2(f) & \cdots & Y_M(f) \end{array}\right]^T \\ &= \mathbf{x}(f) + \mathbf{v}(f) \\ &= \mathbf{d}\left(f, \cos\theta_{\mathrm{d}}\right) X(f) + \mathbf{v}(f), \end{aligned} \tag{1}$$

where $Y_m(f)$ is the mth sensor signal, $\mathbf{x}(f) = \mathbf{d}\left(f, \cos\theta_{\mathrm{d}}\right) X(f)$,

$$\mathbf{d}\left(f, \cos\theta_{\mathrm{d}}\right) = \left[\begin{array}{cccc} 1 & e^{-\jmath 2\pi f \delta \cos\theta_{\mathrm{d}}/c} & \cdots & e^{-\jmath(M-1)2\pi f \delta \cos\theta_{\mathrm{d}}/c} \end{array}\right]^T \tag{2}$$

is the steering vector, $X(f)$ is the desired source signal, and $\mathbf{v}(f)$ is the additive noise signal vector of length M.

To ensure that differential beamforming takes place, the following two assumptions are made [2], [3], [4], [5].

(i) The sensor spacing, δ, is much smaller than the wavelength, $\lambda = c/f$, i.e., $\delta \ll \lambda$ (this implies that $f\delta \ll c$).

(ii) The desired source signal propagates from the angle $\theta_{\mathrm{d}} = 0$ (endfire direction).

Assumption (i) is required so that the true acoustic pressure differentials can be approximated by finite differences of the sensors' outputs.

It also implies that we can well approximate the exponential function in the steering vector with the first few elements of its series expansion; so that frequency-invariant beamforming may be possible.

From Assumption (ii), (1) becomes

$$\mathbf{y}(f) = \mathbf{d}\,(f, 1)\, X(f) + \mathbf{v}(f), \tag{3}$$

and, at the endfire, the value of the beamformer beampattern should always be equal to 1 (or maximal).

With the linear approach, the beamformer output is simply [1]

$$\begin{aligned} Z(f) &= \sum_{m=1}^{M} H_m^*(f) Y_m(f) \\ &= \mathbf{h}^H(f)\mathbf{y}(f) \\ &= \mathbf{h}^H(f)\mathbf{d}\,(f, 1)\, X(f) + \mathbf{h}^H(f)\mathbf{v}(f), \end{aligned} \tag{4}$$

where $Z(f)$ is, in general, the estimate of the desired signal, $X(f)$, and $\mathbf{h}(f)$ is the beamformer of length M.

In our context, the distortionless constraint is desired, i.e.,

$$\mathbf{h}^H(f)\mathbf{d}(f,1) = 1. \tag{5}$$

This means that the value of the beamformer beampattern is equal to 1 at $\theta = 0$ and smaller than 1 at $\theta \neq 0$.

In this talk, we study differential sensor arrays (DSAs) of different orders.

Beampatterns

The beampattern or directivity pattern, which describes the sensitivity of the beamformer to a plane wave impinging on the array from the direction θ, is defined as

$$\mathcal{B}\left[\mathbf{h}(f), \cos\theta\right] = \mathbf{d}^H\left(f, \cos\theta\right)\mathbf{h}(f) \tag{6}$$
$$= \sum_{m=1}^{M} H_m(f) e^{\jmath(m-1)2\pi f \delta \cos\theta / c}.$$

The beampattern of a theoretical Nth-order DSA is defined as [3]

$$\mathcal{B}\left(\mathbf{a}_N, \cos\theta\right) = \sum_{n=0}^{N} a_{N,n} \cos^n\theta = \mathbf{a}_N^T \mathbf{p}\left(\cos\theta\right), \tag{7}$$

where $a_{N,n},\ n = 0, 1, \ldots, N$ are real coefficients and

$$\mathbf{a}_N = \left[\begin{array}{cccc} a_{N,0} & a_{N,1} & \cdots & a_{N,N} \end{array}\right]^T,$$
$$\mathbf{p}\left(\cos\theta\right) = \left[\begin{array}{cccc} 1 & \cos\theta & \cdots & \cos^N\theta \end{array}\right]^T.$$

The different values of the coefficients $a_{N,n},\ n = 0, 1, \ldots, N$ determine the different directivity patterns of the Nth-order DSA.

It may be convenient to use a normalization convention for the coefficients.

For that, in the direction of the desired signal, i.e., for $\theta = 0$, we would like the beampattern to be equal to 1, i.e., $\mathcal{B}\left(\mathbf{a}_N, 1\right) = 1$.

Therefore, we have

$$\sum_{n=0}^{N} a_{N,n} = 1. \tag{8}$$

As a result, we may choose the first coefficient as

$$a_{N,0} = 1 - \sum_{n=1}^{N} a_{N,n}. \tag{9}$$

Since $\cos\theta$ is an even function, so is $\mathcal{B}\left(\mathbf{a}_N, \cos\theta\right)$.

Therefore, on a polar plot, $\mathcal{B}\left(\mathbf{a}_N, \cos\theta\right)$ is symmetric about the axis $0 - \pi$ and any DSA beampattern design can be restricted to this range.

All interesting beampatterns have at least one null in some direction.

It follows from (7) that an Nth-order directivity pattern has at most N (distinct) nulls in this range.

Front-to-Back Ratios

The front-to-back ratio (FBR) is defined as the ratio of the power of the output of the array to signals propagating from the front-half plane to the output power for signals arriving from the rear-half plane [6].

This ratio, for the spherically isotropic (diffuse) noise field, is mathematically defined as [6]

$$\begin{aligned}\mathcal{F}\left[\mathbf{h}(f)\right] &= \frac{\int_0^{\pi/2} \left|\mathcal{B}\left[\mathbf{h}(f), \cos\theta\right]\right|^2 \sin\theta d\theta}{\int_{\pi/2}^{\pi} \left|\mathcal{B}\left[\mathbf{h}(f), \cos\theta\right]\right|^2 \sin\theta d\theta} \\ &= \frac{\mathbf{h}^H(f)\mathbf{\Gamma}_{0,\pi/2}(f)\mathbf{h}(f)}{\mathbf{h}^H(f)\mathbf{\Gamma}_{\pi/2,\pi}(f)\mathbf{h}(f)},\end{aligned} \tag{10}$$

where

$$\mathbf{\Gamma}_{0,\pi/2}(f) = \int_0^{\pi/2} \mathbf{d}\left(f, \cos\theta\right) \mathbf{d}^H\left(f, \cos\theta\right) \sin\theta d\theta, \tag{11}$$

$$\mathbf{\Gamma}_{\pi/2,\pi}(f) = \int_{\pi/2}^{\pi} \mathbf{d}\left(f, \cos\theta\right) \mathbf{d}^H\left(f, \cos\theta\right) \sin\theta d\theta. \tag{12}$$

Now, let us compute the entries of the matrix:

$$\mathbf{\Gamma}_{\psi_1,\psi_2}(f) = \mathcal{N}_{\psi_1,\psi_2} \int_{\psi_1}^{\psi_2} \mathbf{d}\left(f, \cos\theta\right) \mathbf{d}^H\left(f, \cos\theta\right) \sin\theta d\theta, \tag{13}$$

where $0 \leq \psi_1 \leq \psi_2 \leq \pi$ and

$$\mathcal{N}_{\psi_1,\psi_2} = \frac{1}{\int_{\psi_1}^{\psi_2} \sin\theta d\theta} = \frac{1}{\cos\psi_1 - \cos\psi_2} \tag{14}$$

is a normalization term.

The (i,j)th element (with $i,j=1,2,\ldots,M$) of $\mathbf{\Gamma}_{\psi_1,\psi_2}(f)$ can be written as

$$\begin{aligned}
[\mathbf{\Gamma}_{\psi_1,\psi_2}(f)]_{ij} &= \mathcal{N}_{\psi_1,\psi_2}\int_{\psi_1}^{\psi_2} e^{-\jmath 2\pi f(i-1)\tau_0\cos\theta} e^{\jmath 2\pi f(j-1)\tau_0\cos\theta}\sin\theta d\theta \\
&= \mathcal{N}_{\psi_1,\psi_2}\int_{\psi_1}^{\psi_2} e^{\jmath 2\pi f(j-i)\tau_0\cos\theta}\sin\theta d\theta \\
&= -\mathcal{N}_{\psi_1,\psi_2}\int_{\cos\psi_1}^{\cos\psi_2} e^{\jmath 2\pi f(j-i)\tau_0 u} du \\
&= \mathcal{N}_{\psi_1,\psi_2}\int_{\cos\psi_2}^{\cos\psi_1} e^{\jmath 2\pi f(j-i)\tau_0 u} du, \qquad (15)
\end{aligned}$$

where $\tau_0 = \delta/c$.

Therefore, we deduce that

$$[\mathbf{\Gamma}_{\psi_1,\psi_2}(f)]_{ij} = \mathcal{N}_{\psi_1,\psi_2} \frac{e^{\jmath 2\pi f(j-i)\tau_0 \cos\psi_1} - e^{\jmath 2\pi f(j-i)\tau_0 \cos\psi_2}}{\jmath 2\pi f(j-i)\tau_0}, \quad (16)$$

with $[\mathbf{\Gamma}_{\psi_1,\psi_2}(f)]_{mm} = 1,\ m = 1, 2, \ldots, M.$

As a result, the elements of the $M \times M$ matrices $\mathbf{\Gamma}_{0,\pi/2}(f)$ and $\mathbf{\Gamma}_{\pi/2,\pi}(f)$ are, respectively,

$$\left[\mathbf{\Gamma}_{0,\pi/2}(f)\right]_{ij} = \frac{e^{\jmath 2\pi f(j-i)\tau_0} - 1}{\jmath 2\pi f(j-i)\tau_0} \quad (17)$$

$$\left[\mathbf{\Gamma}_{\pi/2,\pi}(f)\right]_{ij} = \frac{1 - e^{-\jmath 2\pi f(j-i)\tau_0}}{\jmath 2\pi f(j-i)\tau_0}, \quad (18)$$

with $\left[\mathbf{\Gamma}_{0,\pi/2}(f)\right]_{mm} = \left[\mathbf{\Gamma}_{\pi/2,\pi}(f)\right]_{mm} = 1,\ m = 1, 2, \ldots, M.$

For the spherically isotropic noise field, the frequency-independent FBR of a theoretical Nth-order DSA is defined as [3]

$$\mathcal{F}\left(\mathbf{a}_N\right) = \frac{\int_0^{\pi/2} \mathcal{B}^2\left(\mathbf{a}_N, \cos\theta\right) \sin\theta d\theta}{\int_{\pi/2}^{\pi} \mathcal{B}^2\left(\mathbf{a}_N, \cos\theta\right) \sin\theta d\theta}. \tag{19}$$

Array Gains

The array gain is given by

$$\mathcal{G}\left[\mathbf{h}(f)\right] = \frac{\left|\mathbf{h}^H(f)\mathbf{d}\left(f,1\right)\right|^2}{\mathbf{h}^H(f)\mathbf{\Gamma_v}(f)\mathbf{h}(f)}, \tag{20}$$

where $\mathbf{\Gamma_v}(f)$ is the pseudo-coherence matrix of $\mathbf{v}(f)$.

The WNG is directly deduced from (20) by taking $\mathbf{\Gamma_v}(f) = \mathbf{I}_M$.

We obtain

$$\mathcal{W}\left[\mathbf{h}(f)\right] = \frac{\left|\mathbf{h}^H(f)\mathbf{d}\left(f,1\right)\right|^2}{\mathbf{h}^H(f)\mathbf{h}(f)} \tag{21}$$

and we can easily show that the maximum WNG is

$$\mathcal{W}_{\max} = M. \tag{22}$$

The DF, which is the array gain in the diffuse (spherically isotropic) noise field, is given by

$$\mathcal{D}\left[\mathbf{h}(f)\right] = \frac{\left|\mathbf{h}^H(f)\mathbf{d}\left(f,1\right)\right|^2}{\mathbf{h}^H(f)\mathbf{\Gamma}_{0,\pi}(f)\mathbf{h}(f)} \tag{23}$$

and the maximum DF is

$$\mathcal{D}_{\max}(f) = \mathbf{d}^H\left(f,1\right)\mathbf{\Gamma}_{0,\pi}^{-1}(f)\mathbf{d}\left(f,1\right). \tag{24}$$

We also have

$$\lim_{\delta\to 0}\mathcal{D}_{\max}(f) = M^2. \tag{25}$$

For the spherically isotropic noise field, the frequency-independent DF of a theoretical Nth-order DSA is defined as [3]

$$\mathcal{D}\left(\mathbf{a}_N\right) = \frac{\mathcal{B}^2\left(\mathbf{a}_N, 1\right)}{\frac{1}{2}\int_0^{\pi} \mathcal{B}^2\left(\mathbf{a}_N, \cos\theta\right) \sin\theta d\theta}. \tag{26}$$

Differential Beamformers

Nth-Order Differential Beamformers

The most well-known and studied Nth-order DSA beampatterns are the dipole, the cardioid, the hypercardioid, and the supercardioid.

In the following, we show how they are obtained.

The Nth-order dipole has a unique null with multiplicity N in the direction $\pi/2$.

Its beampattern is then given by

$$\mathcal{B}_{N,\mathrm{Dp}}\left(\cos\theta\right) = \cos^N\theta, \tag{27}$$

implying that $a_{N,N} = 1$ and $a_{N,N-1} = a_{N,N-2} = \cdots = a_{N,0} = 0$.

The Nth-order cardioid has a unique null with multiplicity N in the direction π.

Its beampattern is then given by

$$\begin{aligned}\mathcal{B}_{N,\mathrm{Cd}}\left(\cos\theta\right) &= \frac{1}{2^N}\left(1+\cos\theta\right)^N \\ &= \sum_{n=0}^{N}\frac{N!}{2^N n!(N-n)!}\cos^n\theta,\end{aligned} \tag{28}$$

implying that

$$a_{N,n} = \frac{N!}{2^N n!(N-n)!},\ n=0,1,\ldots,N. \tag{29}$$

The coefficients of the Nth-order hypercardioid can be obtained by maximizing the DF, $\mathcal{D}(\mathbf{a}_N)$, given in (26).

It can be shown that [3]

$$\mathcal{D}(\mathbf{a}_N) = \frac{\mathbf{a}_N^T \mathbf{1}\mathbf{1}^T \mathbf{a}_N}{\mathbf{a}_N^T \mathbf{H}_N \mathbf{a}_N}, \tag{30}$$

where $\mathbf{1} = \begin{bmatrix} 1 & 1 & \cdots & 1 \end{bmatrix}^T$ is a vector of length $N+1$ and $\mathbf{H}_N$ is a Hankel matrix [of size $(N+1)\times(N+1)$] whose elements are given by

$$[\mathbf{H}_N]_{ij} = \begin{cases} \dfrac{1}{1+i+j}, & \text{if } i+j \text{ even} \\ 0, & \text{otherwise} \end{cases}, \tag{31}$$

with $i, j = 0, 1, \ldots, N$.

In (30), we notice the generalized Rayleigh quotient.

Therefore, the vector $\mathbf{a}_N$ that maximizes $\mathcal{D}(\mathbf{a}_N)$ is the eigenvector corresponding to the maximum eigenvalue of the matrix $\mathbf{H}_N^{-1}\mathbf{1}\mathbf{1}^T$, i.e.,

$$\mathbf{a}_{N,\max} = \frac{\mathbf{H}_N^{-1}\mathbf{1}}{\mathbf{1}^T\mathbf{H}_N^{-1}\mathbf{1}}. \tag{32}$$

As a result, the beampattern of the Nth-order hypercardioid is

$$\mathcal{B}_{N,\mathrm{Hd}}(\cos\theta) = \frac{\mathbf{1}^T\mathbf{H}_N^{-1}\mathbf{p}(\cos\theta)}{\mathbf{1}^T\mathbf{H}_N^{-1}\mathbf{1}}. \tag{33}$$

The coefficients of the Nth-order supercardioid can be obtained by maximizing the FBR, $\mathcal{F}(\mathbf{a}_N)$, defined in (19).

It can be shown that [3]

$$\mathcal{F}(\mathbf{a}_N) = \frac{\mathbf{a}_N^T \mathbf{H}_N'' \mathbf{a}_N}{\mathbf{a}_N^T \mathbf{H}_N' \mathbf{a}_N}, \tag{34}$$

where $\mathbf{H}_N'$ and $\mathbf{H}_N''$ are two Hankel matrices [of size $(N+1) \times (N+1)$] whose elements are given by, respectively,

$$[\mathbf{H}_N']_{ij} = \frac{(-1)^{i+j}}{1+i+j} \tag{35}$$

and

$$[\mathbf{H}_N'']_{ij} = \frac{1}{1+i+j}, \tag{36}$$

with $i, j = 0, 1, \ldots, N$.

Let us denote by $\mathbf{a}'_{N,\max}$ the eigenvector corresponding to the maximum eigenvalue of $\mathbf{H}'^{-1}_N \mathbf{H}''_N$.

Then, $\mathbf{a}'_{N,\max}$ maximizes the FBR and the beampattern of the Nth-order supercardioid is

$$\mathcal{B}_{N,\mathrm{Sd}}\left(\cos\theta\right) = \frac{\mathbf{a}'^T_{N,\max}\mathbf{p}\left(\cos\theta\right)}{\mathbf{a}'^T_{N,\max}\mathbf{p}\left(1\right)}. \tag{37}$$

The most well-known first-order directivity patterns are expressed as

$$\mathcal{B}_{1,\mathrm{Dp}}\left(\cos\theta\right) = \cos\theta, \tag{38}$$

$$\mathcal{B}_{1,\mathrm{Cd}}\left(\cos\theta\right) = \frac{1}{2} + \frac{1}{2}\cos\theta, \tag{39}$$

$$\mathcal{B}_{1,\mathrm{Hd}}\left(\cos\theta\right) = \frac{1}{4} + \frac{3}{4}\cos\theta, \tag{40}$$

$$\mathcal{B}_{1,\mathrm{Sd}}\left(\cos\theta\right) = \frac{\sqrt{3}-1}{2} + \frac{3-\sqrt{3}}{2}\cos\theta. \tag{41}$$

Figure 2 shows these different polar beampatterns.

What is exactly shown are the values of the magnitude squared beampattern in dB, i.e., $10\log_{10}\mathcal{B}^2\left(\mathbf{a}_N, \cos\theta\right)$.

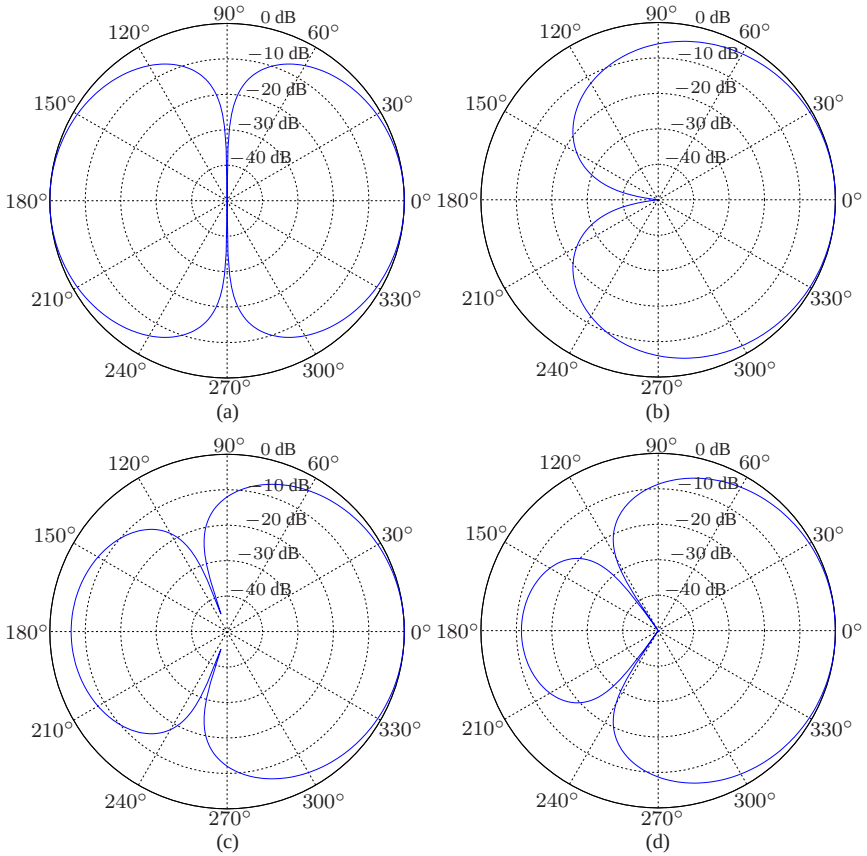

Figure 2: First-order directivity patterns: (a) dipole, (b) cardioid, (c) hypercardioid, and (d) supercardioid.

The most interesting second-order directivity patterns are given by

$$\mathcal{B}_{2,\mathrm{Dp}}\left(\cos\theta\right) = \cos^2\theta, \tag{42}$$

$$\mathcal{B}_{2,\mathrm{Cd}}\left(\cos\theta\right) = \frac{1}{4} + \frac{1}{2}\cos\theta + \frac{1}{4}\cos^2\theta, \tag{43}$$

$$\mathcal{B}_{2,\mathrm{Hd}}\left(\cos\theta\right) = -\frac{1}{6} + \frac{1}{3}\cos\theta + \frac{5}{6}\cos^2\theta, \tag{44}$$

$$\mathcal{B}_{2,\mathrm{Sd}}\left(\cos\theta\right) = \frac{1}{2\left(3+\sqrt{7}\right)} + \frac{\sqrt{7}}{3+\sqrt{7}}\cos\theta + \frac{5}{2\left(3+\sqrt{7}\right)}\cos^2\theta. \tag{45}$$

Figure 3 depicts the different second-order directivity patterns given above.

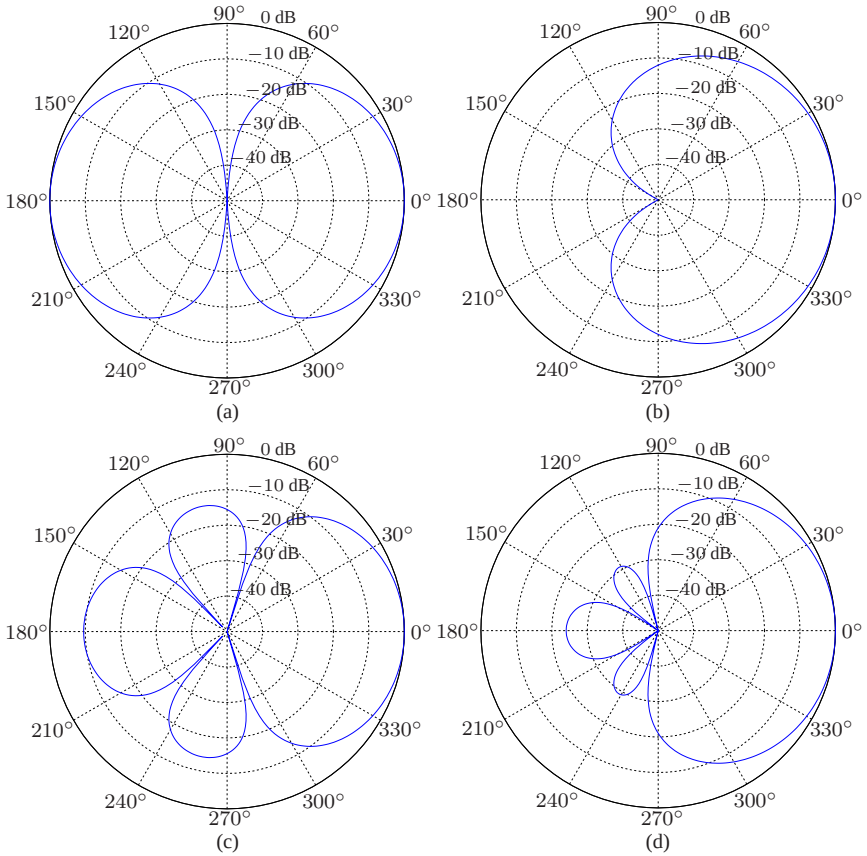

Figure 3: Second-order directivity patterns: (a) dipole, (b) cardioid, (c) hypercardioid, and (d) supercardioid.

The most important third-order directivity patterns are expressed as

$$\mathcal{B}_{3,\mathrm{Dp}}(\cos\theta) = \cos^3\theta, \tag{46}$$

$$\mathcal{B}_{3,\mathrm{Cd}}(\cos\theta) = \frac{1}{8} + \frac{3}{8}\cos\theta + \frac{3}{8}\cos^2\theta + \frac{1}{8}\cos^3\theta, \tag{47}$$

$$\mathcal{B}_{3,\mathrm{Hd}}(\cos\theta) = -\frac{3}{32} - \frac{15}{32}\cos\theta + \frac{15}{32}\cos^2\theta + \frac{35}{32}\cos^3\theta, \tag{48}$$

$$\mathcal{B}_{3,\mathrm{Sd}}(\cos\theta) \approx 0.0184 + 0.2004\cos\theta + 0.4750\cos^2\theta + 0.3061\cos^3\theta. \tag{49}$$

Figure 4 depicts the different third-order directivity patterns given above.

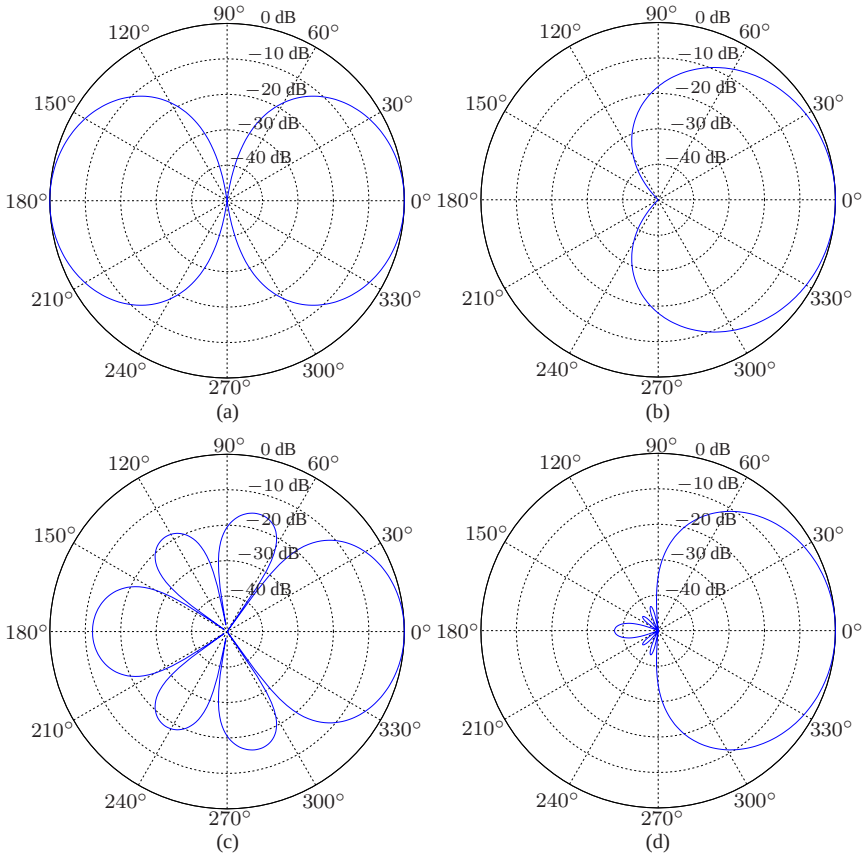

Figure 4: Third-order directivity patterns: (a) dipole, (b) cardioid, (c) hypercardioid, and (d) supercardioid.

The proposed approach to design DSAs is based, mostly, on the obvious observation that any interesting theoretical frequency-independent DSA beampattern has a one at the angle $\theta = 0$ and a number of nulls in some specific directions (with $\theta \gg 0$).

In the most obvious design, which is also the conventional way to do differential beamforming, the number of sensors is equal to the order plus one, i.e., $M = N + 1$.

First-Order Design

First-order DSAs are designed with two sensors.

In this case, we have exactly two constraints to fulfill.

The first constraint is the distortionless response (a one at the angle $\theta = 0$) and the second constraint is a null in the interval $0 < \theta \leq \pi$.

Thus, these two constraints can be written as

$$\mathbf{d}^H(f, 1)\,\mathbf{h}(f) = 1, \tag{50}$$

$$\mathbf{d}^H(f, \alpha_{1,1})\,\mathbf{h}(f) = 0, \tag{51}$$

where $\alpha_{1,1} = \cos\theta_{1,1}$ is given by design (a null at the angle $\theta_{1,1}$) with $-1 \leq \alpha_{1,1} < 1$.

We can express (50)–(51) as

$$\begin{bmatrix} \mathbf{d}^H(f,1) \\ \mathbf{d}^H(f,\alpha_{1,1}) \end{bmatrix} \mathbf{h}(f) = \begin{bmatrix} 1 & e^{\jmath 2\pi f \tau_0} \\ 1 & e^{\jmath 2\pi f \tau_0 \alpha_{1,1}} \end{bmatrix} \mathbf{h}(f) = \begin{bmatrix} 1 \\ 0 \end{bmatrix}. \tag{52}$$

The previous expression is a linear system of two equations and two unknowns for which the solution is

$$\mathbf{h}_1(f) = \frac{1}{1 - e^{\jmath 2\pi f \tau_0 (1-\alpha_{1,1})}} \begin{bmatrix} 1 \\ -e^{-\jmath 2\pi f \tau_0 \alpha_{1,1}} \end{bmatrix}. \tag{53}$$

Substituting (53) into (6), we find that the beampattern is

$$\mathcal{B}\left[\mathbf{h}_1(f), \cos\theta\right] = \frac{1 - e^{\jmath 2\pi f \tau_0 (\cos\theta - \alpha_{1,1})}}{1 - e^{\jmath 2\pi f \tau_0 (1-\alpha_{1,1})}}. \tag{54}$$

Using Assumption (i) and the approximation:

$$e^x \approx 1 + x, \tag{55}$$

we can approximate (54) as

$$\mathcal{B}\left[\mathbf{h}_1(f), \cos\theta\right] \approx \frac{1}{1-\alpha_{1,1}}\cos\theta - \frac{\alpha_{1,1}}{1-\alpha_{1,1}}, \tag{56}$$

which resembles the theoretical first-order DSA.

Most importantly, the beampattern is frequency invariant, which is important in applications dealing with broadband signals such as speech.

It is not hard to find that the DF is

$$\mathcal{D}\left[\mathbf{h}_1(f)\right] = \frac{1-\cos\left[2\pi f\tau_0\left(1-\alpha_{1,1}\right)\right]}{1-\operatorname{sinc}\left(2\pi f\tau_0\right)\cos\left(2\pi f\tau_0\alpha_{1,1}\right)}. \tag{57}$$

Using the approximations:

$$\cos x \approx 1 - \frac{x^2}{2}, \quad \operatorname{sinc} x \approx 1 - \frac{x^2}{6}, \tag{58}$$

the DF becomes

$$\mathcal{D}\left[\mathbf{h}_1(f)\right] \approx \frac{\left(1-\alpha_{1,1}\right)^2}{\alpha_{1,1}^2 + \frac{1}{3}}. \tag{59}$$

We observe that the DF is almost frequency independent as long as δ is small.

Also, the value of $\alpha_{1,1}$ that maximizes (59) is equal to $-1/3$, which corresponds to the hypercardioid and leads to a DF of 4; this is the maximum possible DF for $M = 2$.

The WNG is

$$\begin{aligned}\mathcal{W}\left[\mathbf{h}_1(f)\right] &= \frac{1}{2}\left|1 - e^{\jmath 2\pi f \tau_0 (1-\alpha_{1,1})}\right|^2 \\ &= 1 - \cos\left[2\pi f \tau_0 \left(1 - \alpha_{1,1}\right)\right],\end{aligned} \tag{60}$$

which we can approximate as

$$\mathcal{W}\left[\mathbf{h}_1(f)\right] \approx \frac{1}{2}\left[2\pi f \tau_0 \left(1 - \alpha_{1,1}\right)\right]^2. \tag{61}$$

Observations regarding the WNG:

- very much frequency dependent,
- much larger at high than at low frequencies,
- can be smaller than 1, especially at low frequencies, implying white noise amplification,
- maximized for $\alpha_{1,1} = -1$, which corresponds to the cardioid.

Design Examples

In this section, important particular cases of first-order DSAs with two sensors are numerically studied.

Depending on the value of $\alpha_{1,1}$ we find four interesting first-order DSAs.

- Dipole: $\alpha_{1,1} = 0$.
- Cardioid: $\alpha_{1,1} = -1$.
- Hypercardioid: $\alpha_{1,1} = -\frac{1}{3}$.
- Supercardioid: $\alpha_{1,1} = \frac{1-\sqrt{3}}{3-\sqrt{3}}$.

Figure 5 displays the patterns [with $\mathbf{h}_1(f)$ defined in (53)] of the first-order dipole, cardioid, hypercardioid, and supercardioid for a low frequency ($f = 0.5$ kHz) and a small value of δ ($\delta = 1$ cm).

Figure 6 shows the patterns for a high frequency ($f = 7$ kHz) and a small value of δ ($\delta = 1$ cm).

As long as the sensor spacing is small, the beampatterns of the first-order DSAs are frequency independent.

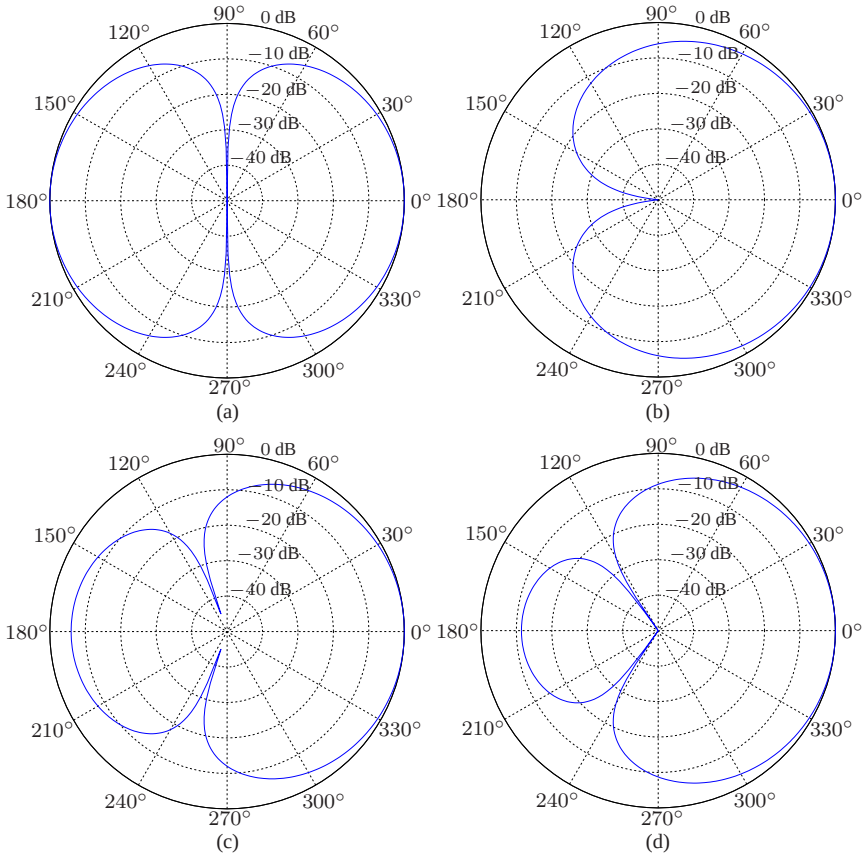

Figure 5: Beampatterns of the first-order DSAs for $f = 0.5$ kHz and $\delta = 1$ cm: (a) dipole, (b) cardioid, (c) hypercardioid, and (d) supercardioid.

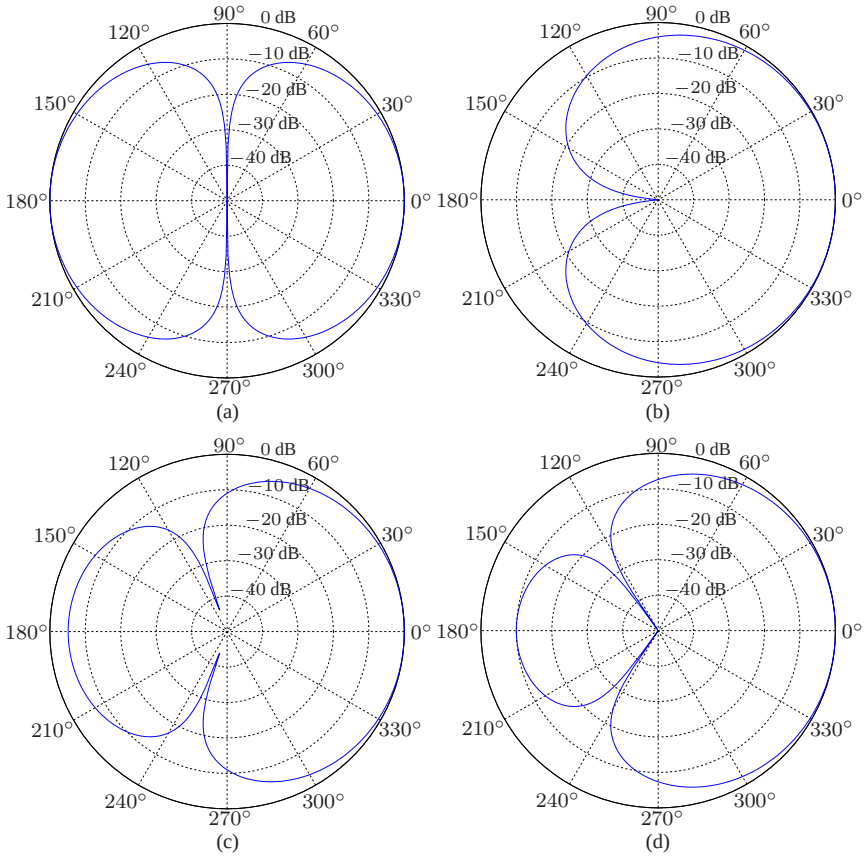

Figure 6: Beampatterns of the first-order DSAs for $f = 7$ kHz and $\delta = 1$ cm: (a) dipole, (b) cardioid, (c) hypercardioid, and (d) supercardioid.

Figures 7 and 8 display the patterns of the first-order dipole, cardioid, hypercardioid, and supercardioid for a value of δ equal to 4 cm.

In this case, the sensor spacing is too large, which causes deterioration of the beampatterns at high frequencies.

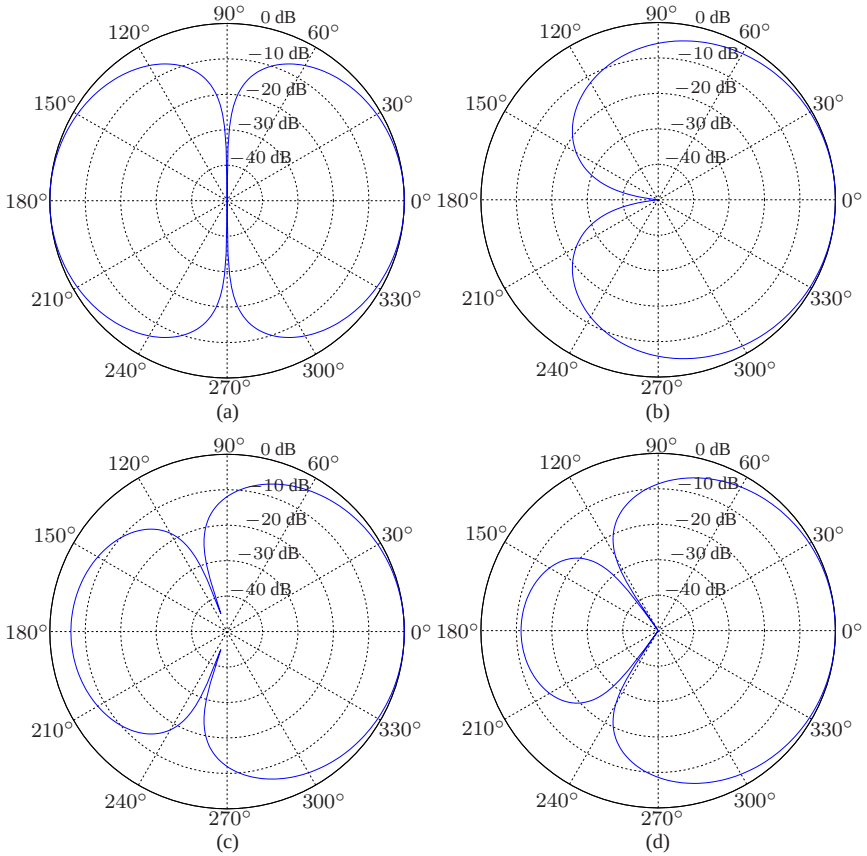

Figure 7: Beampatterns of the first-order DSAs for $f = 0.5$ kHz and $\delta = 4$ cm: (a) dipole, (b) cardioid, (c) hypercardioid, and (d) supercardioid.

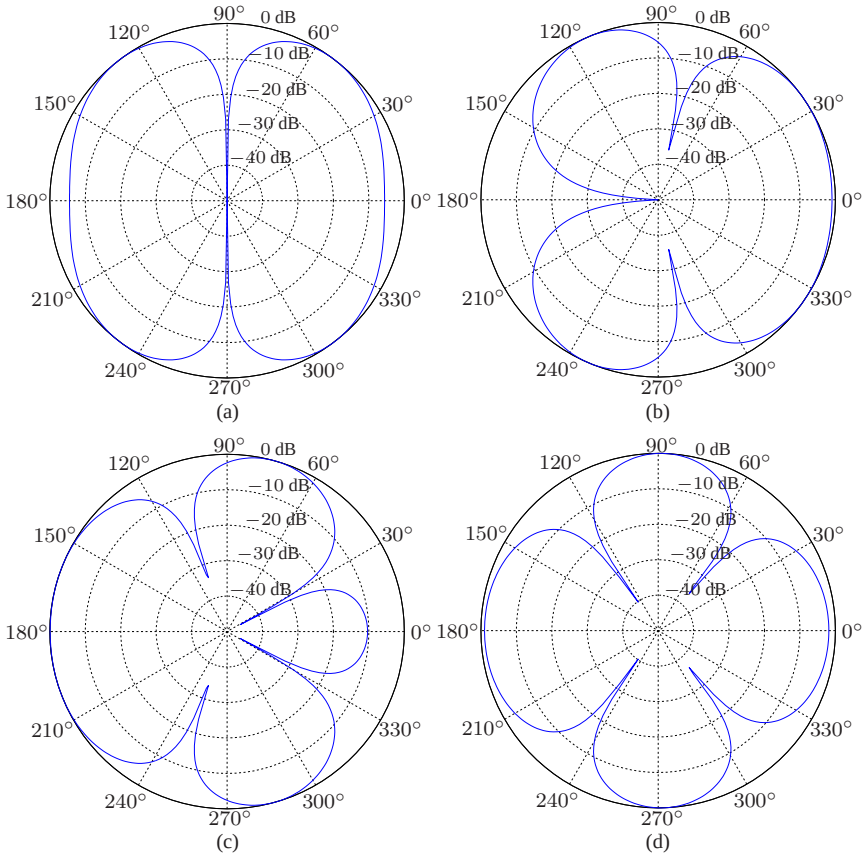

Figure 8: Beampatterns of the first-order DSAs for $f = 7$ kHz and $\delta = 4$ cm: (a) dipole, (b) cardioid, (c) hypercardioid, and (d) supercardioid.

Figure 9 shows plots of the DF, $\mathcal{D}\left[\mathbf{h}_1(f)\right]$, for the dipole, cardioid, hypercardioid, and supercardioid and several values of δ.

Corresponding plots of the WNG, $\mathcal{W}\left[\mathbf{h}_1(f)\right]$ are depicted in Fig. 10.

We observe that increasing δ enables to increase the WNG, especially at low frequencies.

However, a large δ is in contradiction with the DSA assumption.

Therefore, δ should be selected according to the compromise between white noise amplification at low frequencies, and frequency-independent directivity pattern at high frequencies.

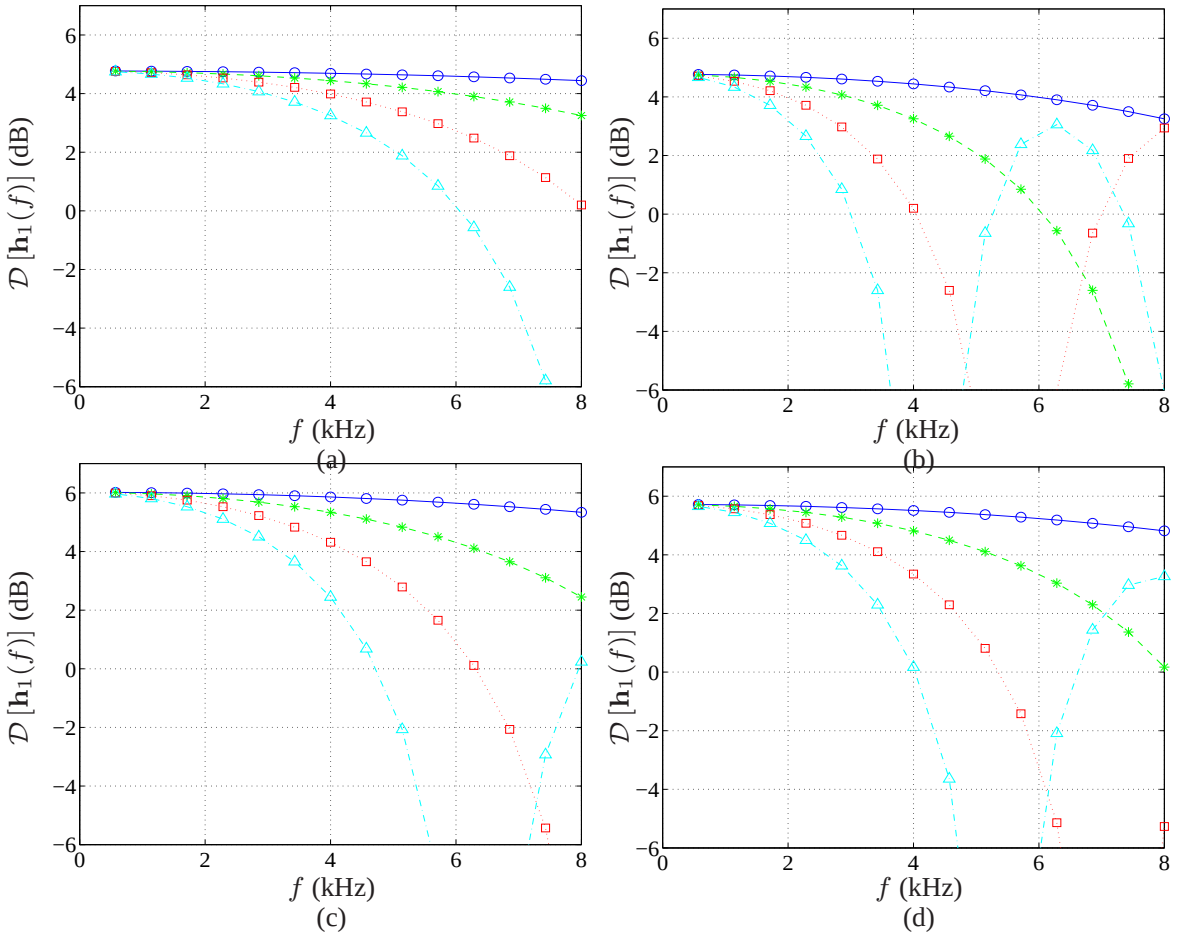

Figure 9: DF of the first-order DSAs as a function of frequency, for several values of δ: $\delta = 1$ cm (solid line with circles), $\delta = 2$ cm (dashed line with asterisks), $\delta = 3$ cm (dotted line with squares), and $\delta = 4$ cm (dash-dot line with triangles). (a) Dipole, (b) cardioid, (c) hypercardioid, and (d) supercardioid.

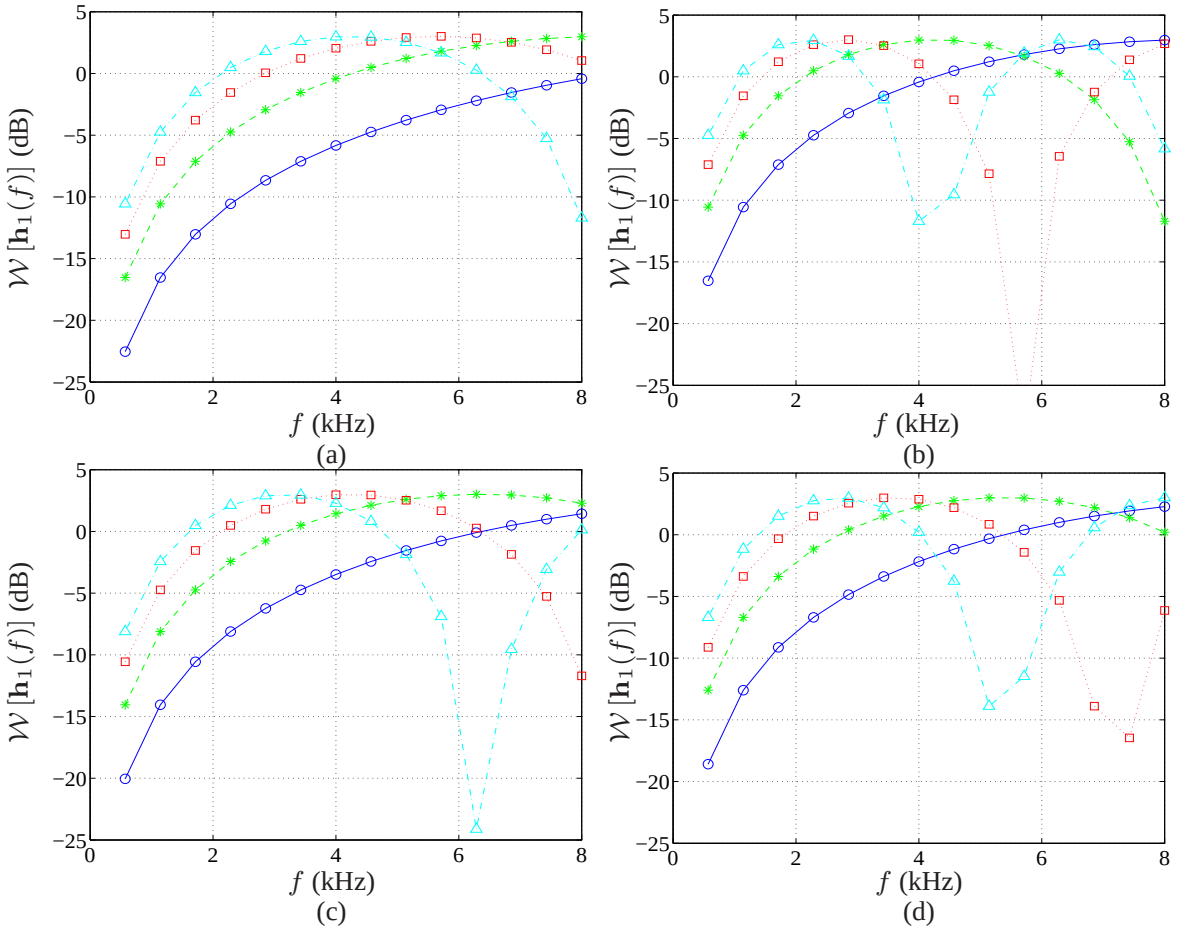

Figure 10: WNG of the first-order DSAs as a function of frequency, for several values of δ: $\delta = 1$ cm (solid line with circles), $\delta = 2$ cm (dashed line with asterisks), $\delta = 3$ cm (dotted line with squares), and $\delta = 4$ cm (dash-dot line with triangles). (a) Dipole, (b) cardioid, (c) hypercardioid, and (d) supercardioid.

Second-Order Design

Any second-order DSA can be realized with three sensors.

Therefore, we assume that we have exactly three sensors.

As a result, we have three constraints to fulfill with the first one being, as usual, a one at the angle $\theta = 0$.

We deduce that the general linear system of equations to design any second-order differential array is

$$\begin{bmatrix} \mathbf{d}^H(f,1) \\ \mathbf{d}^H(f,\alpha_{2,1}) \\ \mathbf{d}^H(f,\alpha_{2,2}) \end{bmatrix} \mathbf{h}(f) = \begin{bmatrix} 1 \\ \beta_{2,1} \\ \beta_{2,2} \end{bmatrix}, \tag{62}$$

where $-1 \leq \alpha_{2,1} = \cos\theta_{2,1} < 1$, $-1 \leq \alpha_{2,2} = \cos\theta_{2,2} < 1$, $\alpha_{2,1} \neq \alpha_{2,2}$, $-1 \leq \beta_{2,1} \leq 1$, and $-1 \leq \beta_{2,2} \leq 1$.

The parameter $\alpha_{2,i}$ is a chosen direction and $\beta_{2,i}$ is its corresponding value on the given desired beampattern.

We should always privilege the zeroes of the beampattern.

Let us denote by

$$\begin{aligned}\mathbf{V}(f) &= \begin{bmatrix} \mathbf{d}^H(f,1) \\ \mathbf{d}^H(f,\alpha_{2,1}) \\ \mathbf{d}^H(f,\alpha_{2,2}) \end{bmatrix} \\ &= \begin{bmatrix} 1 & v_1(f) & v_1^2(f) \\ 1 & v_2(f) & v_2^2(f) \\ 1 & v_3(f) & v_3^2(f) \end{bmatrix}\end{aligned} \tag{63}$$

the 3×3 Vandermonde matrix that appears in (62), where $v_1(f) = e^{\jmath 2\pi f \tau_0}$, $v_2(f) = e^{\jmath 2\pi f \tau_0 \alpha_{2,1}}$, and $v_3(f) = e^{\jmath 2\pi f \tau_0 \alpha_{2,2}}$.

From the decomposition $\mathbf{V}^{-1}(f) = \mathbf{U}(f)\mathbf{L}(f)$ [4], where

$$\mathbf{U}(f) = \begin{bmatrix} 1 & -v_1(f) & v_1(f)v_2(f) \\ 0 & 1 & -[v_1(f) + v_2(f)] \\ 0 & 0 & 1 \end{bmatrix} \tag{64}$$

and (note that in some matrices, we drop the dependency on f to simplify the presentation)

$$\mathbf{L}(f) = \begin{bmatrix} 1 & \dfrac{1}{v_2 - v_1} & 0 \\ \dfrac{1}{v_1 - v_2} & 1 & 0 \\ \dfrac{1}{(v_1 - v_2)(v_1 - v_3)} & \dfrac{1}{(v_2 - v_1)(v_2 - v_3)} & \dfrac{1}{(v_3 - v_1)(v_3 - v_2)} \end{bmatrix}, \tag{65}$$

we find that the inverse of $\mathbf{V}(f)$ is

$$\mathbf{V}^{-1}(f) = \begin{bmatrix} \dfrac{v_2 v_3}{(v_2 - v_1)(v_3 - v_1)} & -\dfrac{v_1 v_3}{(v_2 - v_1)(v_3 - v_2)} & \dfrac{v_1 v_2}{(v_3 - v_1)(v_3 - v_2)} \\ -\dfrac{v_2 + v_3}{(v_2 - v_1)(v_3 - v_1)} & \dfrac{v_1 + v_3}{(v_2 - v_1)(v_3 - v_2)} & -\dfrac{v_1 + v_2}{(v_3 - v_1)(v_3 - v_2)} \\ \dfrac{1}{(v_2 - v_1)(v_3 - v_1)} & -\dfrac{1}{(v_2 - v_1)(v_3 - v_2)} & \dfrac{1}{(v_3 - v_1)(v_3 - v_2)} \end{bmatrix}. \tag{66}$$

This inverse can help to study and design second-order DSAs.

We deduce that the beamformer is

$$\mathbf{h}_2(f) = \mathbf{U}(f)\mathbf{L}(f) \begin{bmatrix} 1 \\ \beta_{2,1} \\ \beta_{2,2} \end{bmatrix}. \tag{67}$$

While the previous approach is very general, it is not concerned by beampatterns that have a zero with multiplicity greater than 1.

Let us show how to design a beampattern that has a zero, $\alpha_{2,1}$, with multiplicity 2.

The theoretical DSA beampattern of such a case is

$$\mathcal{B}\left(\alpha_{2,1},\alpha\right)=\frac{1}{\left(1-\alpha_{2,1}\right)^{2}}\left(\alpha-\alpha_{2,1}\right)^{2}, \tag{68}$$

where $\alpha=\cos\theta$.

It is clear that the derivative of $\mathcal{B}\left(\alpha_{2,1},\alpha\right)$ with respect to α at $\alpha_{2,1}$ is

$$\left.\frac{d\mathcal{B}\left(\alpha_{2,1},\alpha\right)}{d\alpha}\right|_{\alpha=\alpha_{2,1}}=0. \tag{69}$$

Applying this property to the beamformer beampattern, we get

$$\left.\frac{d\mathcal{B}\left[\mathbf{h}(f),\alpha\right]}{d\alpha}\right|_{\alpha=\alpha_{2,1}} = \jmath 2\pi f \tau_0 \left[\boldsymbol{\Sigma}\mathbf{d}\left(f,\alpha_{2,1}\right)\right]^H \mathbf{h}(f) = 0, \tag{70}$$

where $\boldsymbol{\Sigma} = \mathrm{diag}\left(0,1,2\right)$ is a diagonal matrix.

From (70), we deduce the constraint equation:

$$\left[\boldsymbol{\Sigma}\mathbf{d}\left(f,\alpha_{2,1}\right)\right]^H \mathbf{h}(f) = 0. \tag{71}$$

Combining the distortionless constraint, the null constraint in the direction $\alpha_{2,1}$, i.e., $\mathbf{d}\left(f,\alpha_{2,1}\right)\mathbf{h}(f) = 0$, and (71), we obtain

$$\begin{bmatrix} \mathbf{d}^H\left(f,1\right) \\ \mathbf{d}^H\left(f,\alpha_{2,1}\right) \\ \left[\boldsymbol{\Sigma}\mathbf{d}\left(f,\alpha_{2,1}\right)\right]^H \end{bmatrix} \mathbf{h}(f) = \begin{bmatrix} 1 \\ 0 \\ 0 \end{bmatrix}. \tag{72}$$

It is straightforward to see that the solution is

$$\mathbf{h}_{2,0}(f) = \frac{1}{\left[1 - e^{\jmath 2\pi f \tau_0 (1-\alpha_{2,1})}\right]^2} \begin{bmatrix} 1 \\ -2e^{-\jmath 2\pi f \tau_0 \alpha_{2,1}} \\ e^{-\jmath 4\pi f \tau_0 \alpha_{2,1}} \end{bmatrix}. \tag{73}$$

Because of the different particular constraints, it is obvious that the beampattern has the form:

$$\mathcal{B}\left[\mathbf{h}_{2,0}(f), \cos\theta\right] = \frac{\left[1 - e^{\jmath 2\pi f \tau_0 (\cos\theta - \alpha_{2,1})}\right]^2}{\left[1 - e^{\jmath 2\pi f \tau_0 (1-\alpha_{2,1})}\right]^2}. \tag{74}$$

With Assumption (i) and the approximation in (55), we have

$$\mathcal{B}\left[\mathbf{h}_{2,0}(f), \cos\theta\right] \approx \frac{1}{\left(1 - \alpha_{2,1}\right)^2} \left(\cos\theta - \alpha_{2,1}\right)^2. \tag{75}$$

We find that the WNG is

$$\begin{aligned}\mathcal{W}\left[\mathbf{h}_{2,0}(f)\right] &= \frac{1}{6}\left|1-e^{\jmath 2\pi f\tau_0(1-\alpha_{2,1})}\right|^4 \\ &= \frac{2}{3}\left\{1-\cos\left[2\pi f\tau_0\left(1-\alpha_{2,1}\right)\right]\right\}^2,\end{aligned} \tag{76}$$

which can be approximated as

$$\mathcal{W}\left[\mathbf{h}_{2,0}(f)\right] \approx \frac{1}{6}\left[2\pi f\tau_0\left(1-\alpha_{2,1}\right)\right]^4. \tag{77}$$

The WNG of the beamformer with the second-order design is much worse than the WNG of the beamformer with the first-order design.

Design Examples

In this section, we design and compare two second-order DSAs.

The first is a second-order cardioid with $\mathbf{h}_{2,0}(f)$ and $\alpha_{2,1} = -1$, that has a unique multiple null at $\theta = \pi$.

The second DSA is a second-order cardioid with $\mathbf{h}_2(f)$, $\alpha_{2,1} = -1,\ \beta_{2,1} = 0$, $\alpha_{2,2} = 0,\ \beta_{2,2} = 0$, that has two distinct nulls at $\theta = \frac{\pi}{2}$ and π.

Figures 11 and 12 display the patterns of the two second-order cardioids for low and high frequencies and two values of δ.

As long as δ is small, the beampatterns of the second-order DSAs are frequency independent.

When δ is too large, the beampatterns at high frequencies deteriorate.

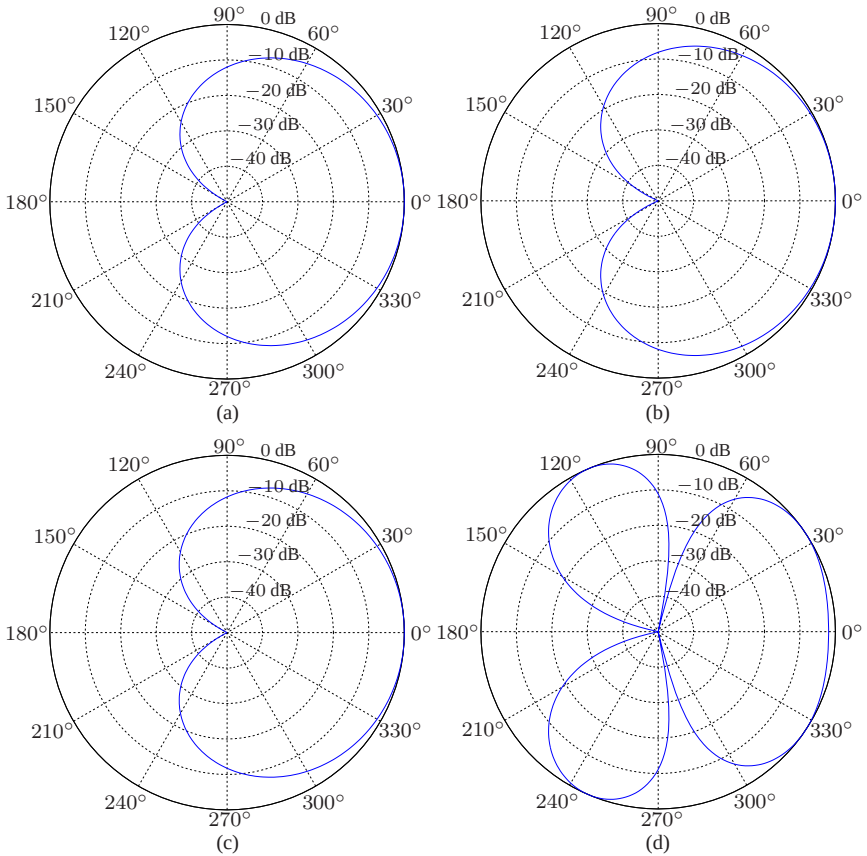

Figure 11: Beampatterns of the second-order cardioid, $\mathbf{h}_{2,0}(f)$, with a unique multiple null at $\theta = \pi$, for low and high frequencies, and two values of δ: (a) $f = 0.5$ kHz, $\delta = 1$ cm, (b) $f = 7$ kHz, $\delta = 1$ cm, (c) $f = 0.5$ kHz, $\delta = 4$ cm, and (d) $f = 7$ kHz, $\delta = 4$ cm.

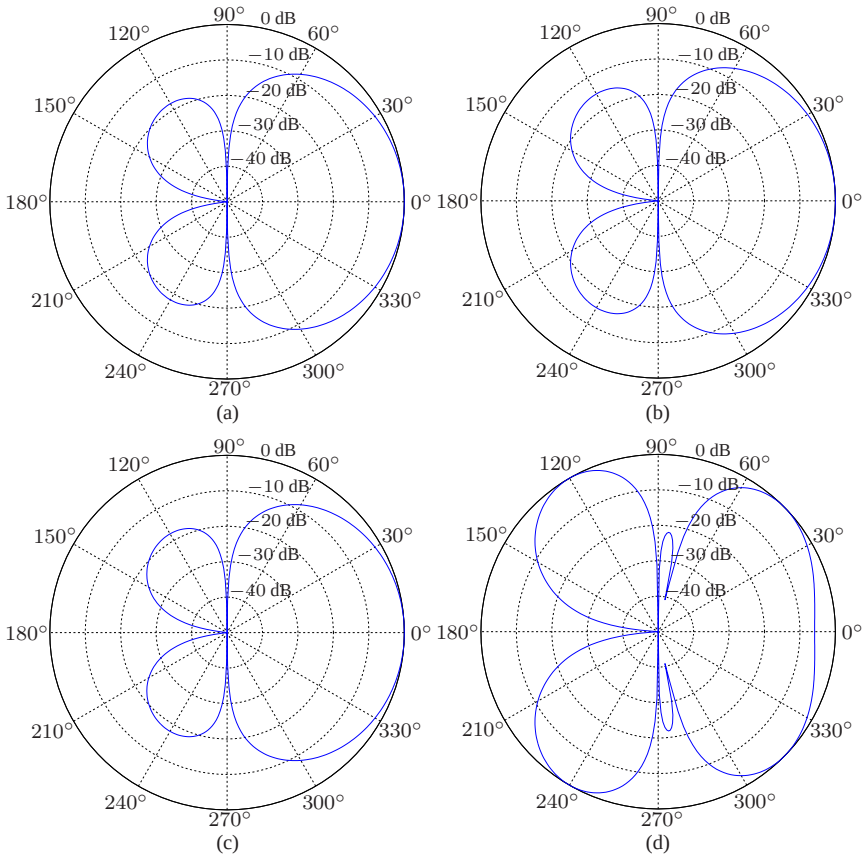

Figure 12: Beampatterns of the second-order cardioid, $\mathbf{h}_2(f)$, with two distinct nulls at $\theta = \frac{\pi}{2}$ and π, for low and high frequencies, and two values of δ: (a) $f = 0.5$ kHz, $\delta = 1$ cm, (b) $f = 7$ kHz, $\delta = 1$ cm, (c) $f = 0.5$ kHz, $\delta = 4$ cm, and (d) $f = 7$ kHz, $\delta = 4$ cm.

Figure 13 shows plots of the DFs of the two second-order cardioids, $\mathcal{D}\left[\mathbf{h}_{2,0}(f)\right]$ and $\mathcal{D}\left[\mathbf{h}_{2}(f)\right]$ for several values of δ.

Corresponding plots of the WNG are depicted in Fig. 14.

We observe that $\mathcal{D}\left[\mathbf{h}_{2}(f)\right]$ is higher than $\mathcal{D}\left[\mathbf{h}_{2,0}(f)\right]$, but at the expense of lower WNG.

Furthermore, similar to the first-order DSAs, increasing δ enables to increase the WNG, especially at low frequencies.

However, a large δ is in contradiction with the DSA assumption.

Therefore, δ should be selected according to the compromise between white noise amplification at low frequencies and frequency-independent directivity pattern at high frequencies.

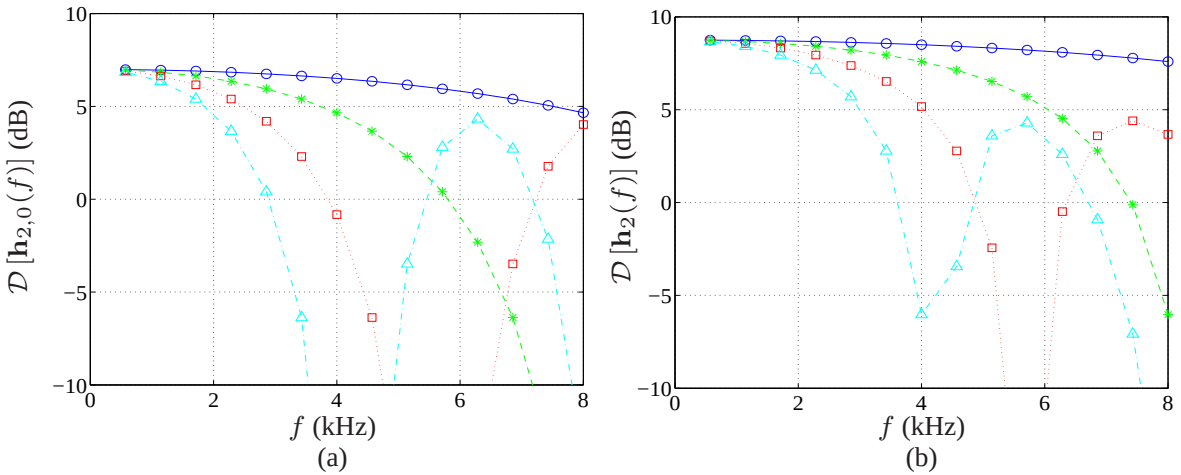

Figure 13: DF of second-order DSAs as a function of frequency, for several values of δ: $\delta = 1$ cm (solid line with circles), $\delta = 2$ cm (dashed line with asterisks), $\delta = 3$ cm (dotted line with squares), and $\delta = 4$ cm (dash-dot line with triangles). (a) Second-order cardioid, $\mathbf{h}_{2,0}(f)$, with a unique multiple null at $\theta = \pi$, and (b) second-order cardioid, $\mathbf{h}_{2}(f)$, with two distinct nulls at $\theta = \frac{\pi}{2}$ and π.

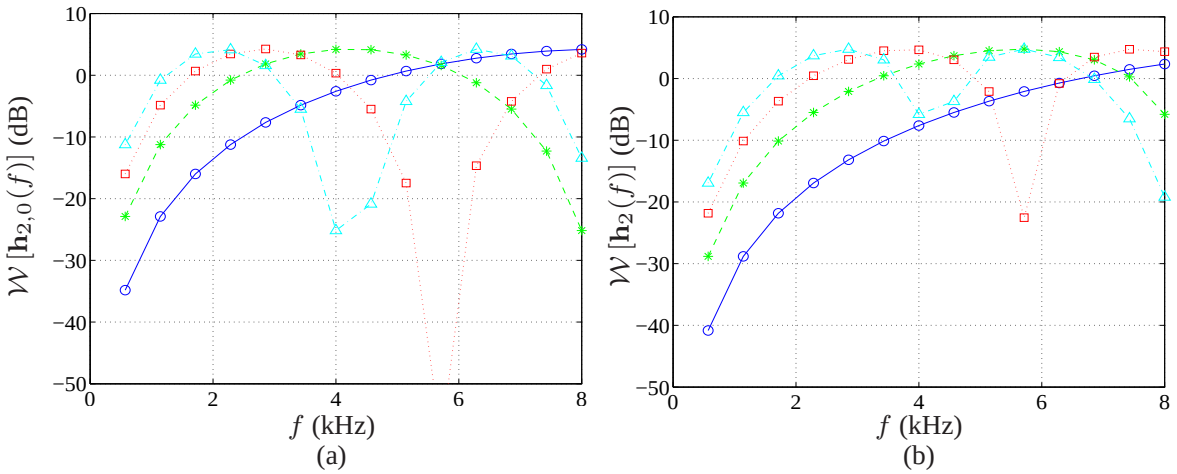

Figure 14: WNG of second-order DSAs as a function of frequency, for several values of δ: $\delta = 1$ cm (solid line with circles), $\delta = 2$ cm (dashed line with asterisks), $\delta = 3$ cm (dotted line with squares), and $\delta = 4$ cm (dash-dot line with triangles). (a) Second-order cardioid, $\mathbf{h}_{2,0}(f)$, with a unique multiple null at $\theta = \pi$, and (b) second-order cardioid, $\mathbf{h}_{2}(f)$, with two distinct nulls at $\theta = \frac{\pi}{2}$ and π.

Third-Order Design

We start this part by deriving an important family of third-order differential beamformers whose beampatterns have three distinct nulls.

This can be done with exactly four omnidirectional sensors.

It is clear that the linear system of four equations tailored for the derivation of such beamformers is

$$\begin{bmatrix} \mathbf{d}^H(f,1) \\ \mathbf{d}^H(f,\alpha_{3,1}) \\ \mathbf{d}^H(f,\alpha_{3,2}) \\ \mathbf{d}^H(f,\alpha_{3,3}) \end{bmatrix} \mathbf{h}(f) = \begin{bmatrix} 1 \\ 0 \\ 0 \\ 0 \end{bmatrix}, \tag{78}$$

where $-1 \leq \alpha_{3,1} = \cos\theta_{3,1} < 1$, $-1 \leq \alpha_{3,2} = \cos\theta_{3,2} < 1$, $-1 \leq \alpha_{3,3} = \cos\theta_{3,3} < 1$, and $\alpha_{3,1} \neq \alpha_{3,2} \neq \alpha_{3,3}$.

We denote by

$$\mathbf{V}(f) = \begin{bmatrix} \mathbf{d}^H(f,1) \\ \mathbf{d}^H(f,\alpha_{3,1}) \\ \mathbf{d}^H(f,\alpha_{3,2}) \\ \mathbf{d}^H(f,\alpha_{3,3}) \end{bmatrix} = \begin{bmatrix} 1 & v_1(f) & v_1^2(f) & v_1^3(f) \\ 1 & v_2(f) & v_2^2(f) & v_2^3(f) \\ 1 & v_3(f) & v_3^2(f) & v_3^3(f) \\ 1 & v_4(f) & v_4^2(f) & v_4^3(f) \end{bmatrix} \tag{79}$$

the 4×4 Vandermonde matrix that appears in (78), where $v_1(f) = e^{\jmath 2\pi f \tau_0}$, $v_2(f) = e^{\jmath 2\pi f \tau_0 \alpha_{3,1}}$, $v_3(f) = e^{\jmath 2\pi f \tau_0 \alpha_{3,2}}$, and $v_4(f) = e^{\jmath 2\pi f \tau_0 \alpha_{3,3}}$.

Because of the structure of the vector on the right-hand side of (78), we only need to compute the first column of $\mathbf{V}^{-1}(f)$ to find $\mathbf{h}(f)$.

Using the decomposition $\mathbf{V}^{-1}(f) = \mathbf{U}(f)\mathbf{L}(f)$ [4], the matrix $\mathbf{U}(f)$, and the first column of $\mathbf{L}(f)$, we find that the first column of $\mathbf{V}^{-1}(f)$ is

$$\mathbf{V}^{-1}(f;:,1) = \begin{bmatrix} \dfrac{v_2 v_3 v_4}{(v_2 - v_1)(v_3 - v_1)(v_4 - v_1)} \\ -\dfrac{v_2 v_3 + v_3 v_4 + v_2 v_4}{(v_2 - v_1)(v_3 - v_1)(v_4 - v_1)} \\ \dfrac{v_2 + v_3 + v_4}{(v_2 - v_1)(v_3 - v_1)(v_4 - v_1)} \\ -\dfrac{1}{(v_2 - v_1)(v_3 - v_1)(v_4 - v_1)} \end{bmatrix}. \tag{80}$$

From the previous expression, we easily find that the solution is

$$\mathbf{h}_3(f) = \frac{1}{\left[1 - e^{\jmath 2\pi f \tau_0 (1-\alpha_{3,1})}\right]\left[1 - e^{\jmath 2\pi f \tau_0 (1-\alpha_{3,2})}\right]\left[1 - e^{\jmath 2\pi f \tau_0 (1-\alpha_{3,3})}\right]} \times \begin{bmatrix} 1 \\ -e^{-\jmath 2\pi f \tau_0 \alpha_{3,1}} - e^{-\jmath 2\pi f \tau_0 \alpha_{3,2}} - e^{-\jmath 2\pi f \tau_0 \alpha_{3,3}} \\ e^{-\jmath 2\pi f \tau_0 (\alpha_{3,1}+\alpha_{3,2})} + e^{-\jmath 2\pi f \tau_0 (\alpha_{3,2}+\alpha_{3,3})} + e^{-\jmath 2\pi f \tau_0 (\alpha_{3,1}+\alpha_{3,3})} \\ -e^{-\jmath 2\pi f \tau_0 (\alpha_{3,1}+\alpha_{3,2}+\alpha_{3,3})} \end{bmatrix}. \quad (81)$$

Now, let us derive differential beamformers whose beampatterns have a unique null in the direction $\alpha_{3,1}$ with multiplicity 3.

Using the facts that

$$\left.\frac{d\mathcal{B}\left[\mathbf{h}(f),\alpha\right]}{d\alpha}\right|_{\alpha=\alpha_{3,1}} = \jmath 2\pi f\tau_0\left[\mathbf{\Sigma d}\left(f,\alpha_{3,1}\right)\right]^H\mathbf{h}(f) = 0 \tag{82}$$

and

$$\left.\frac{d^2\mathcal{B}\left[\mathbf{h}(f),\alpha\right]}{d\alpha^2}\right|_{\alpha=\alpha_{3,1}} = \left(\jmath 2\pi f\tau_0\right)^2\left[\mathbf{\Sigma}^2\mathbf{d}\left(f,\alpha_{3,1}\right)\right]^H\mathbf{h}(f) = 0, \tag{83}$$

where

$$\mathbf{\Sigma} = \mathrm{diag}\left(0,1,2,3\right) \tag{84}$$

is a diagonal matrix, we easily find that the linear system to solve is

$$\begin{bmatrix} \mathbf{d}^H\left(f,1\right) \\ \mathbf{d}^H\left(f,\alpha_{3,1}\right) \\ \left[\mathbf{\Sigma d}\left(f,\alpha_{3,1}\right)\right]^H \\ \left[\mathbf{\Sigma}^2\mathbf{d}\left(f,\alpha_{3,1}\right)\right]^H \end{bmatrix}\mathbf{h}(f) = \begin{bmatrix} 1 \\ 0 \\ 0 \\ 0 \end{bmatrix}. \tag{85}$$

We deduce that the solution is

$$\mathbf{h}_{3,0}(f) = \frac{1}{\left[1 - e^{\jmath 2\pi f \tau_0 (1-\alpha_{3,1})}\right]^3} \begin{bmatrix} 1 \\ -3e^{-\jmath 2\pi f \tau_0 \alpha_{3,1}} \\ 3e^{-\jmath 4\pi f \tau_0 \alpha_{2,1}} \\ -e^{-\jmath 6\pi f \tau_0 \alpha_{2,1}} \end{bmatrix}. \tag{86}$$

The beampattern corresponding to the beamformer $\mathbf{h}_{3,0}(f)$ is

$$\mathcal{B}\left[\mathbf{h}_{3,0}(f), \cos\theta\right] = \frac{\left[1 - e^{\jmath 2\pi f \tau_0 (\cos\theta - \alpha_{3,1})}\right]^3}{\left[1 - e^{\jmath 2\pi f \tau_0 (1-\alpha_{3,1})}\right]^3} \tag{87}$$

and can be approximated as

$$\mathcal{B}\left[\mathbf{h}_{3,0}(f), \cos\theta\right] \approx \frac{1}{\left(1 - \alpha_{3,1}\right)^3} \left(\cos\theta - \alpha_{3,1}\right)^3, \tag{88}$$

which is identical to the theoretical third-order DSA beampattern with a unique null with multiplicity 3.

The WNG is

$$\begin{aligned}\mathcal{W}\left[\mathbf{h}_{3,0}(f)\right] &= \frac{1}{20}\left|1-e^{\jmath 2\pi f\tau_0(1-\alpha_{3,1})}\right|^6 \\ &= \frac{2}{5}\left\{1-\cos\left[2\pi f\tau_0\left(1-\alpha_{3,1}\right)\right]\right\}^3,\end{aligned} \tag{89}$$

which we can approximate as

$$\mathcal{W}\left[\mathbf{h}_{3,0}(f)\right] \approx \frac{1}{20}\left[2\pi f\tau_0\left(1-\alpha_{3,1}\right)\right]^6. \tag{90}$$

The generalization of the beamformers $\mathbf{h}_3(f)$ and $\mathbf{h}_{3,0}(f)$ to any order is straightforward.

It is also possible to derive differential beamformers directly from some of the performance measures.

There are two possibilities.

The first beamformer is obtained by maximizing the DF as defined in (23).

Considering the distortionless constraint, we easily get the hypercardioid of order $M-1$:

$$\mathbf{h}_{\mathrm{Hd}}(f) = \frac{\mathbf{\Gamma}_{0,\pi}^{-1}(f)\mathbf{d}\left(f,1\right)}{\mathbf{d}^{H}\left(f,1\right)\mathbf{\Gamma}_{0,\pi}^{-1}(f)\mathbf{d}\left(f,1\right)}, \tag{91}$$

which is, actually, the superdirective beamformer.

The second differential beamformer is obtained by maximizing the FBR as defined in (10).

If we denote by $\mathbf{t}_1(f)$ the eigenvector corresponding to the maximum eigenvalue of the matrix $\mathbf{\Gamma}_{\pi/2,\pi}^{-1}(f)\mathbf{\Gamma}_{0,\pi/2}(f)$ and taking into account the distortionless constraint, we get the supercardioid of order $M-1$:

$$\mathbf{h}_{\mathrm{Sd}}(f) = \frac{\mathbf{t}_1(f)}{\mathbf{d}^H(f,1)\,\mathbf{t}_1(f)}. \tag{92}$$

Design Examples

In this section, we design and compare four third-order DSAs.

The first is a third-order cardioid with $\mathbf{h}_{3,0}(f)$ and $\alpha_{3,1} = -1$, that has a unique multiple null at $\theta = \pi$.

The second DSA is a third-order DSA with $\mathbf{h}_3(f)$, $\alpha_{3,1} = 0$, $\alpha_{3,2} = -\frac{1}{2}$, and $\alpha_{3,3} = -1$, that has three distinct nulls at $\theta = \frac{\pi}{2}$, $\frac{2\pi}{3}$ and π.

The third and fourth DSAs are, respectively, the third-order hypercardioid with $\mathbf{h}_{\mathrm{Hd}}(f)$ and the third-order supercardioid with $\mathbf{h}_{\mathrm{Sd}}(f)$.

Figures 15–18 display the patterns of the four third-order DSAs for low and high frequencies and two values of δ.

As long as δ is small, the beampatterns of the third-order DSAs are frequency independent.

When δ is too large, the beampatterns at high frequencies deteriorate.

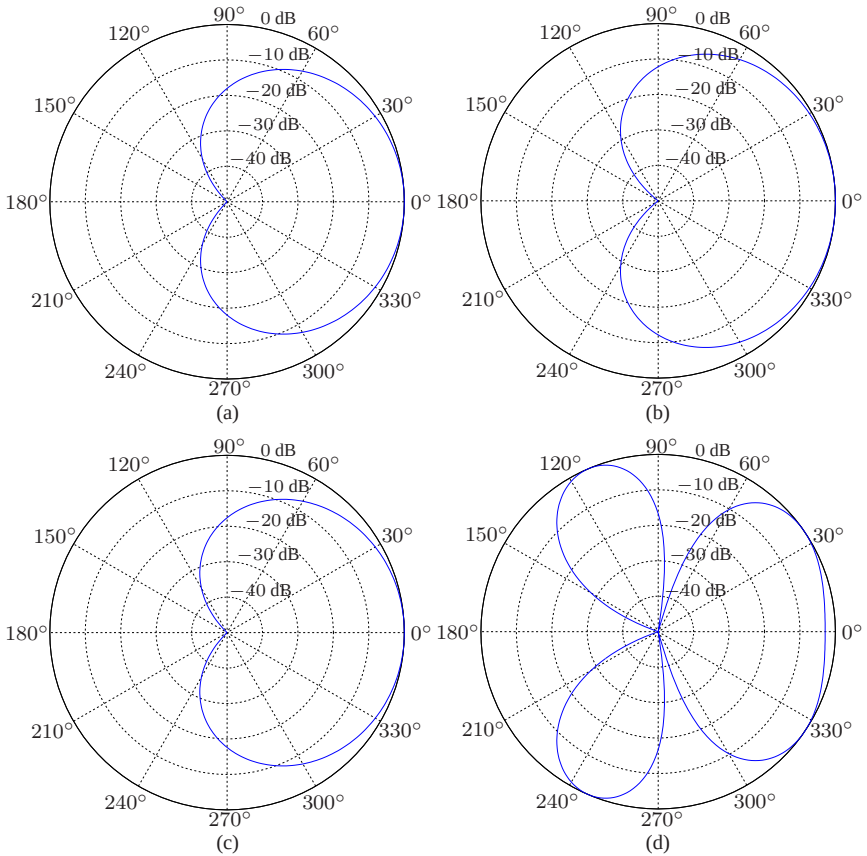

Figure 15: Beampatterns of the third-order cardioid, $\mathbf{h}_{3,0}(f)$, with a unique multiple null at $\theta = \pi$, for low and high frequencies, and two values of δ: (a) $f = 0.5$ kHz, $\delta = 1$ cm, (b) $f = 7$ kHz, $\delta = 1$ cm, (c) $f = 0.5$ kHz, $\delta = 4$ cm, and (d) $f = 7$ kHz, $\delta = 4$ cm.

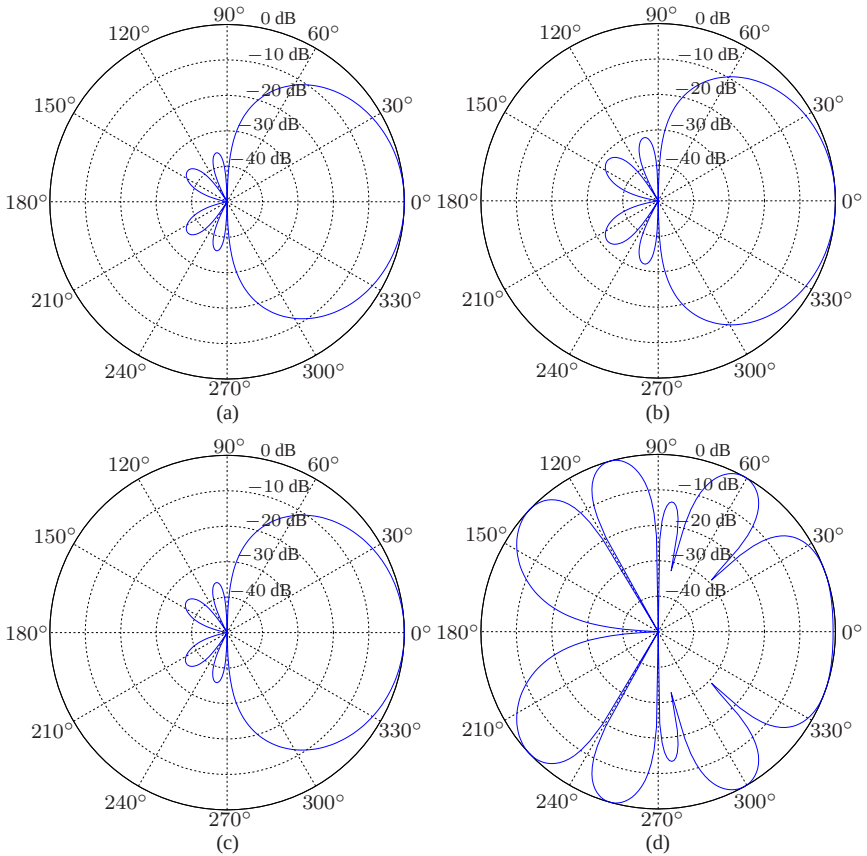

Figure 16: Beampatterns of the third-order DSA, $\mathbf{h}_3(f)$, with three distinct nulls at $\theta = \frac{\pi}{2}, \frac{2\pi}{3}$, and π, for low and high frequencies, and two values of δ: (a) $f = 0.5$ kHz, $\delta = 1$ cm, (b) $f = 7$ kHz, $\delta = 1$ cm, (c) $f = 0.5$ kHz, $\delta = 4$ cm, and (d) $f = 7$ kHz, $\delta = 4$ cm.

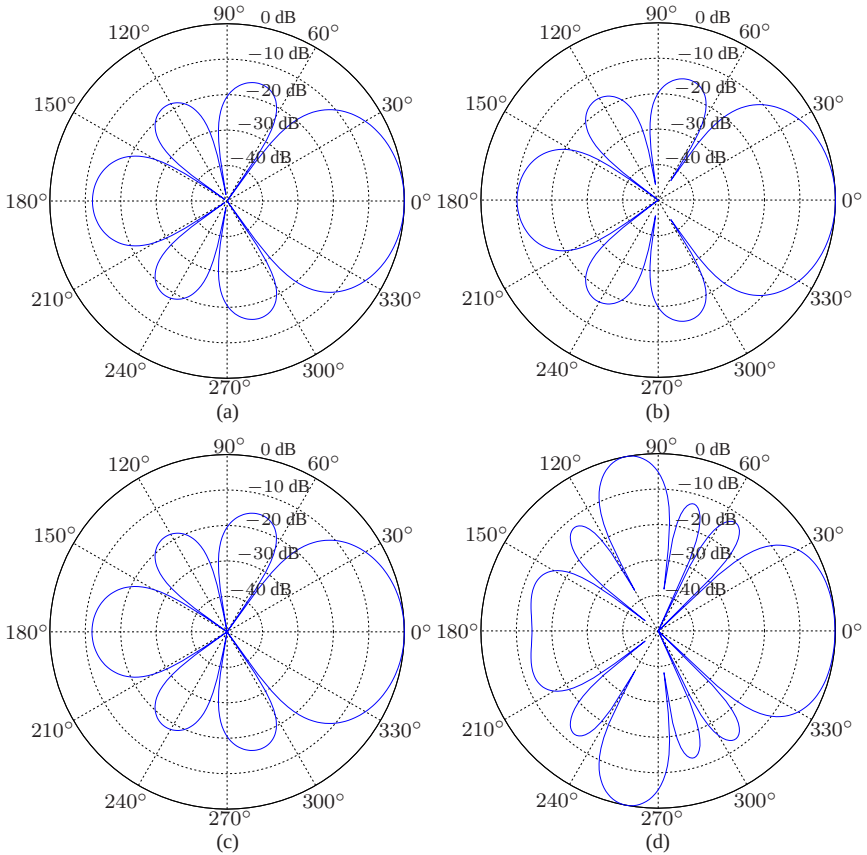

Figure 17: Beampatterns of the third-order hypercardioid, $\mathbf{h}_{\mathrm{Hd}}(f)$, for low and high frequencies, and two values of δ: (a) $f = 0.5$ kHz, $\delta = 1$ cm, (b) $f = 7$ kHz, $\delta = 1$ cm, (c) $f = 0.5$ kHz, $\delta = 4$ cm, and (d) $f = 7$ kHz, $\delta = 4$ cm.

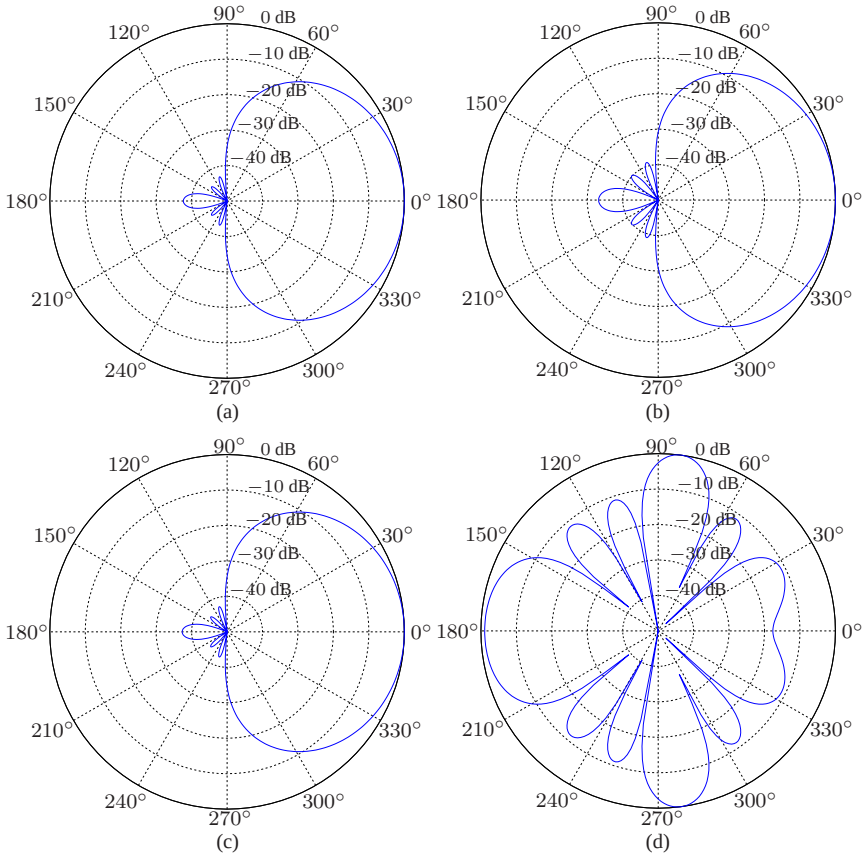

Figure 18: Beampatterns of the third-order supercardioid, $\mathbf{h}_{\mathrm{Sd}}(f)$, for low and high frequencies, and two values of δ: (a) $f = 0.5$ kHz, $\delta = 1$ cm, (b) $f = 7$ kHz, $\delta = 1$ cm, (c) $f = 0.5$ kHz, $\delta = 4$ cm, and (d) $f = 7$ kHz, $\delta = 4$ cm.

Figure 19 shows plots of the DFs of the four third-order DSAs, $\mathcal{D}\left[\mathbf{h}_{3,0}(f)\right]$, $\mathcal{D}\left[\mathbf{h}_{3}(f)\right]$, $\mathcal{D}\left[\mathbf{h}_{\mathrm{Hd}}(f)\right]$, and $\mathcal{D}\left[\mathbf{h}_{\mathrm{Sd}}(f)\right]$, as a function of frequency for several values of δ.

Corresponding plots of the WNG are depicted in Fig. 20.

We observe that the highest DF is obtained with the third-order hypercardioid, but at the cost of the lowest WNG.

The highest WNG is obtained with the third-order cardioid that has a unique multiple null, but at the cost of the lowest DF.

The DF of the third-order cardioid with three distinct nulls is higher than that of the third-order cardioid with a unique multiple null, but at the expense of lower WNG.

Furthermore, similar to the first- and second-order DSAs, increasing δ enables to increase the WNG, especially at low frequencies.

However, a large value of δ is in contradiction with the DSA assumption, which results in deterioration of the beampatterns at high frequencies.

Therefore, the value of δ should be selected according to the compromise between white noise amplification at low frequencies and frequency-independent directivity pattern at high frequencies.

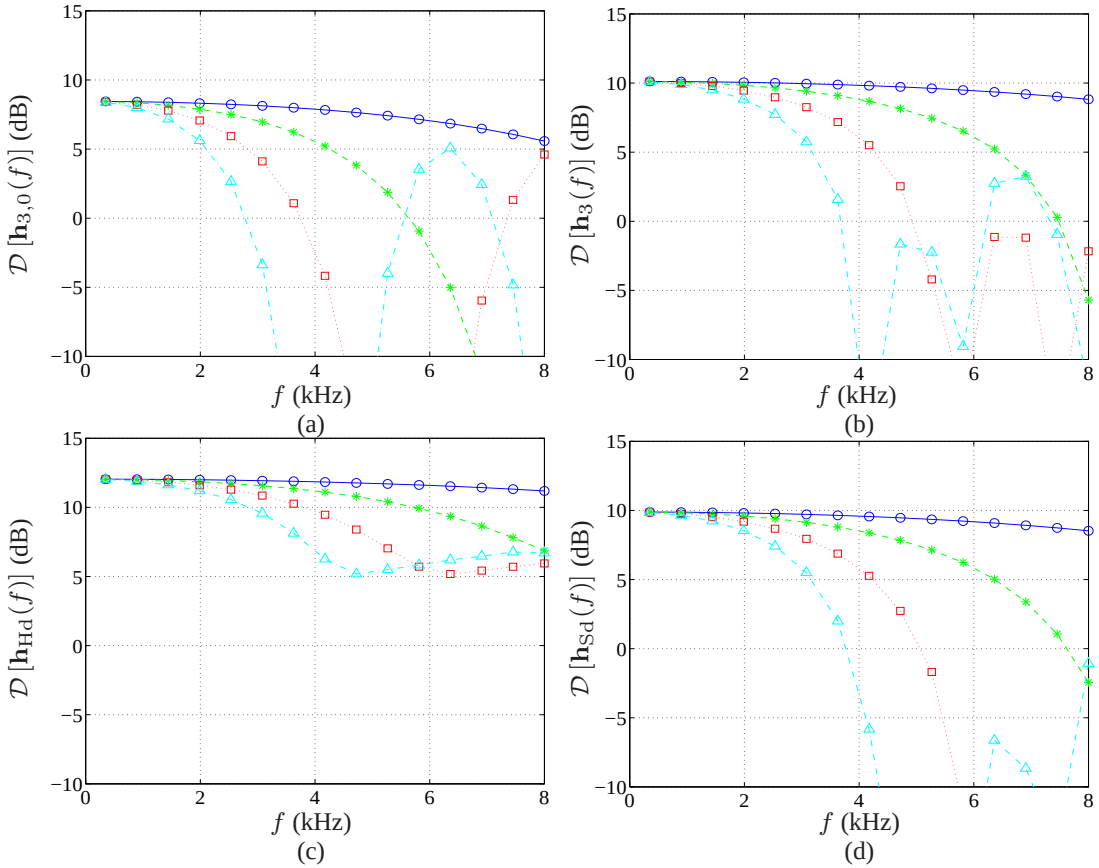

Figure 19: DF of third-order DSAs as a function of frequency for $\delta = 1$ cm (solid line with circles), $\delta = 2$ cm (dashed line with asterisks), $\delta = 3$ cm (dotted line with squares), and $\delta = 4$ cm (dash-dot line with triangles). (a) $\mathbf{h}_{3,0}(f)$, with a multiple null at $\theta = \pi$, (b) $\mathbf{h}_3(f)$, with nulls at $\theta = \frac{\pi}{2}$, $\frac{2\pi}{3}$, and π, (c) $\mathbf{h}_{\mathrm{Hd}}(f)$, and (d) $\mathbf{h}_{\mathrm{Sd}}(f)$.

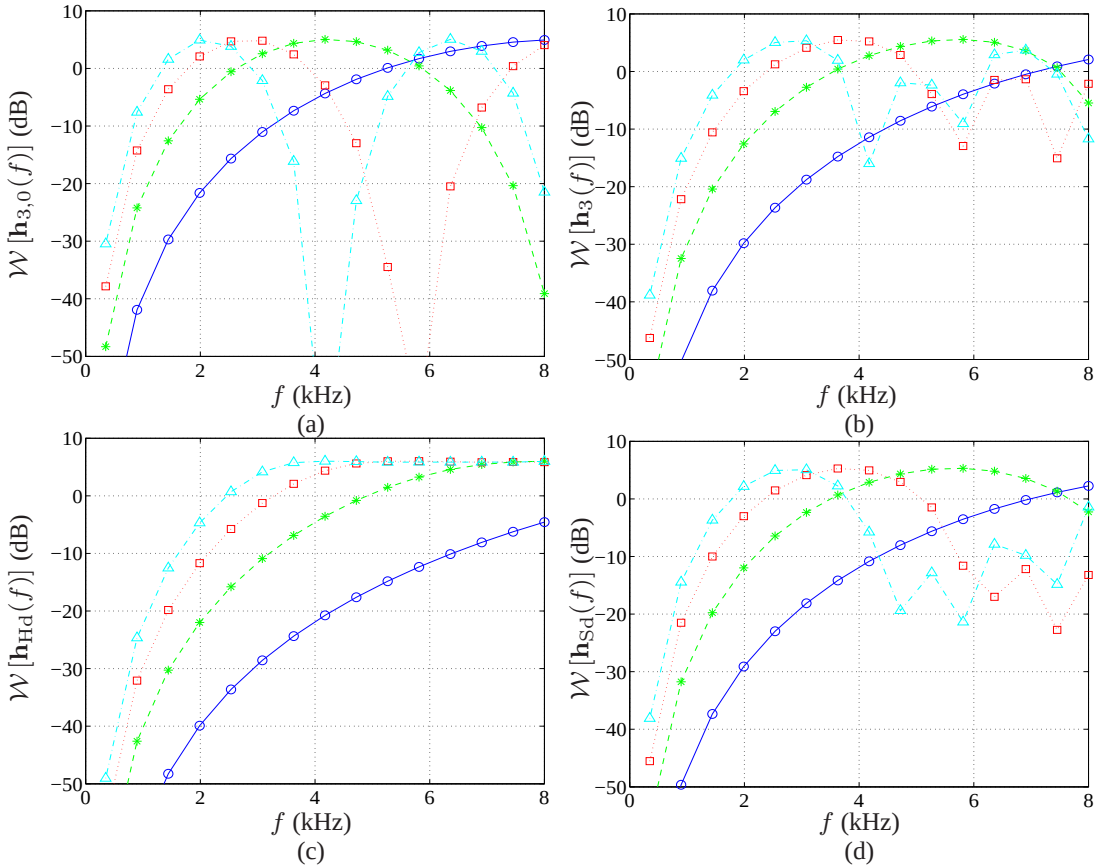

Figure 20: WNG of third-order DSAs as a function of frequency for $\delta = 1$ cm (solid line with circles), $\delta = 2$ cm (dashed line with asterisks), $\delta = 3$ cm (dotted line with squares), and $\delta = 4$ cm (dash-dot line with triangles). (a) $\mathbf{h}_{3,0}(f)$, with a multiple null at $\theta = \pi$, (b) $\mathbf{h}_3(f)$, with nulls at $\theta = \frac{\pi}{2}$, $\frac{2\pi}{3}$, and π, (c) $\mathbf{h}_{\mathrm{Hd}}(f)$, and (d) $\mathbf{h}_{\mathrm{Sd}}(f)$.

Minimum-Norm Beamformers

In the three previous sections, we could observe that the major drawback of DSAs is white noise amplification.

As the order increases, the amplification of white noise worsens.

The best way to deal with this fundamental problem is to unconnect the order of the DSAs from the number of sensors and increase this latter for a fixed order.

Consequently, we could use this degree of freedom to maximize the WNG [4].

We know from the previous sections that any DSA of order N can be designed by solving the linear system of $N+1$ equations:

$$\mathbf{D}\left(f,\boldsymbol{\alpha}\right)\mathbf{h}(f)=\boldsymbol{\beta}, \tag{93}$$

where

$$\mathbf{D}\left(f,\boldsymbol{\alpha}\right)=\begin{bmatrix}\mathbf{d}^{H}\left(f,1\right)\\ \mathbf{d}^{H}\left(f,\alpha_{N,1}\right)\\ \vdots\\ \mathbf{d}^{H}\left(f,\alpha_{N,N}\right)\end{bmatrix} \tag{94}$$

is the constraint matrix of size $(N+1)\times M$,

$$\mathbf{d}\left(f,\alpha_{N,n}\right)=\left[\begin{array}{cccc}1 & e^{-\jmath 2\pi f\tau_0\alpha_{N,n}} & \cdots & e^{-\jmath(M-1)2\pi f\tau_0\alpha_{N,n}}\end{array}\right]^T,$$
$$n=1,2,\ldots,N \tag{95}$$

is a steering vector of length M,

$$\mathbf{h}(f)=\left[\begin{array}{cccc}H_1(f) & H_2(f) & \cdots & H_M(f)\end{array}\right]^T \tag{96}$$

is a filter of length M, and

$$\boldsymbol{\alpha}=\left[\begin{array}{cccc}1 & \alpha_{N,1} & \cdots & \alpha_{N,N}\end{array}\right]^T, \tag{97}$$
$$\boldsymbol{\beta}=\left[\begin{array}{cccc}1 & \beta_{N,1} & \cdots & \beta_{N,N}\end{array}\right]^T, \tag{98}$$

are vectors of length $N+1$ containing the design coefficients of the directivity pattern.

In previous sections, only the case $M = N + 1$ was considered.

This is also the case in all known approaches in the literature [3].

But, obviously from (93), nothing prevents us from taking $M > N + 1$.

Now, assume that $M \geq N + 1$, then we can maximize the WNG subject to (93), i.e.,

$$\min_{\mathbf{h}(f)} \mathbf{h}^H(f)\mathbf{h}(f) \quad \text{subject to} \quad \mathbf{D}\left(f, \boldsymbol{\alpha}\right)\mathbf{h}(f) = \boldsymbol{\beta}. \tag{99}$$

Obviously, the solution of the above problem is

$$\mathbf{h}_{\mathrm{MN}}\left(f, \boldsymbol{\alpha}, \boldsymbol{\beta}\right) = \mathbf{D}^H\left(f, \boldsymbol{\alpha}\right)\left[\mathbf{D}\left(f, \boldsymbol{\alpha}\right)\mathbf{D}^H\left(f, \boldsymbol{\alpha}\right)\right]^{-1}\boldsymbol{\beta}, \tag{100}$$

which is the minimum-norm solution of (93).

The vectors $\boldsymbol{\alpha}$ and $\boldsymbol{\beta}$ of length $N+1$ determine the beampattern and the order of the DSA.

Basically, the length of these vectors determine (roughly) the order of the DSA while their values determine the beampattern.

Meanwhile, the length, M, of the minimum-norm beamformer, $\mathbf{h}_{\mathrm{MN}}(f, \boldsymbol{\alpha}, \boldsymbol{\beta})$, can be much larger than $N+1$, which will help make it robust against white noise amplification.

In this case, the WNG should approach M and the order of the DSA may not be equal to N anymore but the Nth-order DSA fundamental constraints will always be fulfilled.

As a result, the resulting shape of the directivity pattern may slightly be different than the one obtained with $M = N+1$.

It is easy to see that the beampattern, the WNG, and the DF of the minimum-norm beamformer are, respectively,

$$\begin{aligned}\mathcal{B}\left[\mathbf{h}_{\mathrm{MN}}\left(f,\boldsymbol{\alpha},\boldsymbol{\beta}\right),\cos\theta\right] &= \mathbf{d}^{H}\left(f,\cos\theta\right)\mathbf{h}_{\mathrm{MN}}\left(f,\boldsymbol{\alpha},\boldsymbol{\beta}\right) \\ &= \mathbf{d}^{H}\left(f,\cos\theta\right)\mathbf{D}^{H}\left(f,\boldsymbol{\alpha}\right)\left[\mathbf{D}\left(f,\boldsymbol{\alpha}\right)\mathbf{D}^{H}\left(f,\boldsymbol{\alpha}\right)\right]^{-1}\boldsymbol{\beta},\end{aligned} \tag{101}$$

$$\mathcal{W}\left[\mathbf{h}_{\mathrm{MN}}\left(f,\boldsymbol{\alpha},\boldsymbol{\beta}\right)\right] = \frac{1}{\boldsymbol{\beta}^{T}\left[\mathbf{D}\left(f,\boldsymbol{\alpha}\right)\mathbf{D}^{H}\left(f,\boldsymbol{\alpha}\right)\right]^{-1}\boldsymbol{\beta}}, \tag{102}$$

and

$$\mathcal{D}\left[\mathbf{h}_{\mathrm{MN}}\left(f,\boldsymbol{\alpha},\boldsymbol{\beta}\right)\right] = \frac{1}{\mathbf{h}_{\mathrm{MN}}^{H}\left(f,\boldsymbol{\alpha},\boldsymbol{\beta}\right)\boldsymbol{\Gamma}_{0,\pi}(f)\mathbf{h}_{\mathrm{MN}}\left(f,\boldsymbol{\alpha},\boldsymbol{\beta}\right)}. \tag{103}$$

In the same way, we can design a robust DSA whose beampattern has a null in the direction $\alpha_{N,1}$ with multiplicity N.

The constraint equation is

$$\mathbf{D}_0\left(f, \alpha_{N,1}\right)\mathbf{h}(f) = \mathbf{i}_1, \tag{104}$$

where

$$\mathbf{D}_0\left(f, \alpha_{N,1}\right) = \begin{bmatrix} \mathbf{d}^H\left(f, 1\right) \\ \mathbf{d}^H\left(f, \alpha_{N,1}\right) \\ \left[\boldsymbol{\Sigma}\mathbf{d}\left(f, \alpha_{N,1}\right)\right]^H \\ \vdots \\ \left[\boldsymbol{\Sigma}^{N-1}\mathbf{d}\left(f, \alpha_{N,1}\right)\right]^H \end{bmatrix} \tag{105}$$

is a matrix of size $(N+1) \times M$, $\boldsymbol{\Sigma} = \operatorname{diag}\left(0, 1, \ldots, M-1\right)$ is a diagonal matrix, and $\mathbf{i}_1$ is the first column of the $(N+1) \times (N+1)$ identity matrix, $\mathbf{I}_{N+1}$.

Assuming that $M \geq N+1$, the maximization of the WNG subject to (104) leads to the minimum-norm beamformer:

$$\mathbf{h}_{\mathrm{MN},0}\left(f,\alpha_{N,1}\right)=\mathbf{D}_0^H\left(f,\alpha_{N,1}\right)\left[\mathbf{D}_0\left(f,\alpha_{N,1}\right)\mathbf{D}_0^H\left(f,\alpha_{N,1}\right)\right]^{-1}\mathbf{i}_1. \quad (106)$$

Design Examples

In this section, we demonstrate the effectiveness of the minimum-norm filter in the design of robust DSAs.

Fundamentally, we exploit the fact that we have many more sensors than the order of the DSA.

We design and compare two third-order DSAs with different δ.

The first is a a third-order DSA with three distinct nulls with $\mathbf{h}_{\mathrm{MN}}\left(f,\boldsymbol{\alpha},\boldsymbol{\beta}\right)$.

In this scenario, we have

$$\boldsymbol{\alpha} = \begin{bmatrix} 1 & 0 & -\frac{1}{2} & -1 \end{bmatrix}^T, \quad \boldsymbol{\beta} = \begin{bmatrix} 1 & 0 & 0 & 0 \end{bmatrix}^T. \tag{107}$$

The second DSA is a third-order cardioid with $\mathbf{h}_{\mathrm{MN},0}\left(f, \alpha_{3,1}\right)$ and $\alpha_{3,1} = -1$.

In both cases, the interelement spacing is $\delta = 5$ mm.

Figures 21 and 22 display the patterns of the two minimum-norm third-order DSAs for low and high frequencies, and two values of M.

At low frequencies, the patterns for $M = 8$ look similar to the patterns for $M = 4$.

At high frequencies, the patterns for $M = 8$ look less directional than the patterns for $M = 4$.

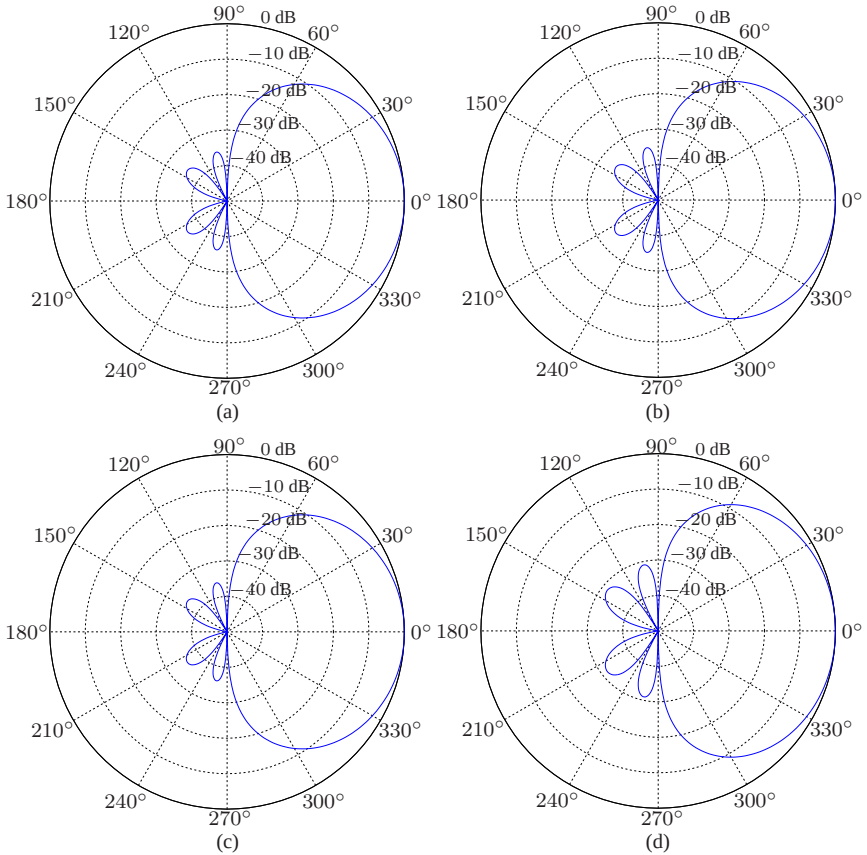

Figure 21: Beampatterns of a third-order DSA with three distinct nulls, $\mathbf{h}_{\mathrm{MN}}(f, \boldsymbol{\alpha}, \boldsymbol{\beta})$, for low and high frequencies, and two values of M: (a) $f = 0.5$ kHz, $M = 4$, (b) $f = 7$ kHz, $M = 4$, (c) $f = 0.5$ kHz, $M = 8$, and (d) $f = 7$ kHz, $M = 8$.

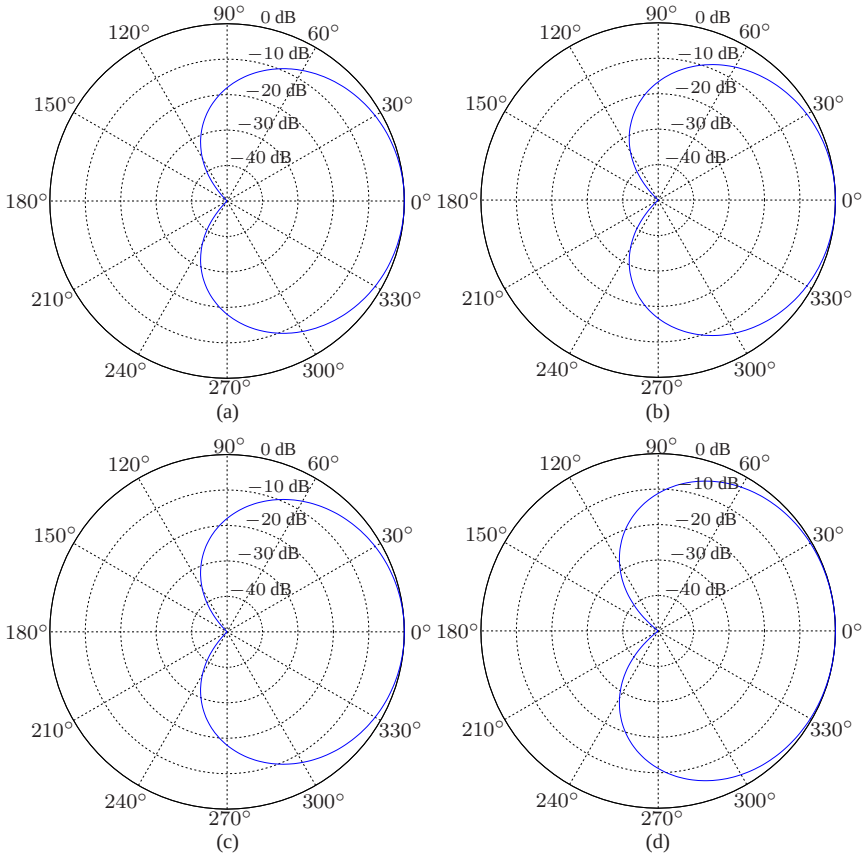

Figure 22: Beampatterns of a third-order cardioid, $\mathbf{h}_{\mathrm{MN},0}(f, \alpha_{3,1})$, with $\alpha_{3,1} = -1$, for low and high frequencies, and two values of M: (a) $f = 0.5$ kHz, $M = 4$, (b) $f = 7$ kHz, $M = 4$, (c) $f = 0.5$ kHz, $M = 8$, and (d) $f = 7$ kHz, $M = 8$.

Figure 23 shows plots of the DFs of the two third-order DSAs, $\mathcal{D}\left[\mathbf{h}_{\mathrm{MN}}\left(f,\boldsymbol{\alpha},\boldsymbol{\beta}\right)\right]$ and $\mathcal{D}\left[\mathbf{h}_{\mathrm{MN},0}\left(f,\alpha_{3,1}\right)\right]$ for several values of M.

Corresponding plots of the WNG are depicted in Fig. 24.

For $M=4$, the DF is almost constant up to 8 kHz.

As M increases, the frequency range for which the DF is constant decreases, but at high frequencies, we can get much higher WNG than at low frequencies.

Increasing M enables to increase the WNG, but the DF at high frequencies decreases.

Furthermore, for a M, the DF $\mathcal{D}\left[\mathbf{h}_{\mathrm{MN}}\left(f,\boldsymbol{\alpha},\boldsymbol{\beta}\right)\right]$ is higher than $\mathcal{D}\left[\mathbf{h}_{\mathrm{MN},0}\left(f,\alpha_{3,1}\right)\right]$, but at the expense of lower WNG.

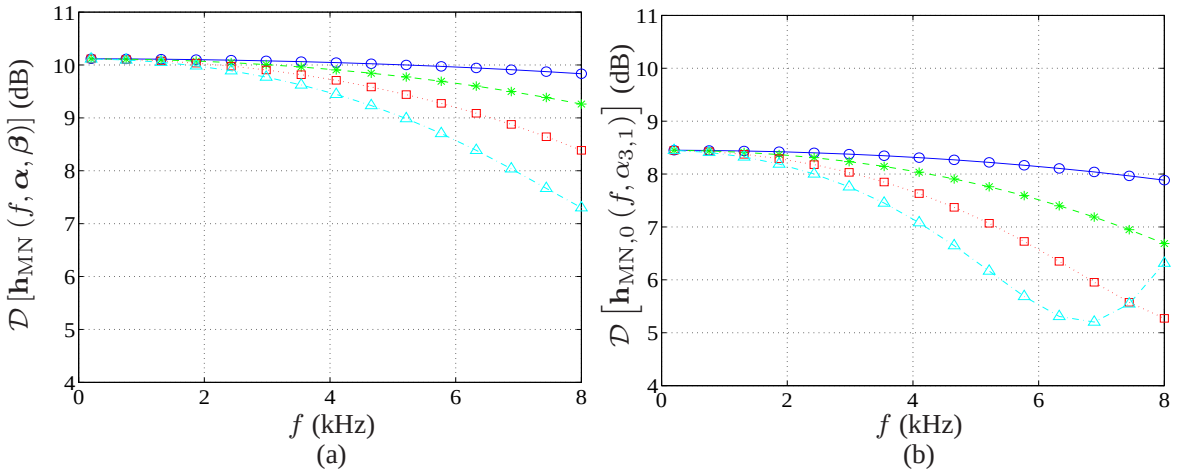

Figure 23: DF of third-order DSAs with minimum-norm filters as a function of frequency, for different values of M: $M = 4$ (solid line with circles), $M = 6$ (dashed line with asterisks), $M = 8$ (dotted line with squares), and $M = 10$ (dash-dot line with triangles). (a) Third-order DSA with three distinct nulls, $\mathbf{h}_{\mathrm{MN}}(f, \boldsymbol{\alpha}, \boldsymbol{\beta})$, and (b) third-order cardioid, $\mathbf{h}_{\mathrm{MN},0}(f, \alpha_{3,1})$, with $\alpha_{3,1} = -1$.

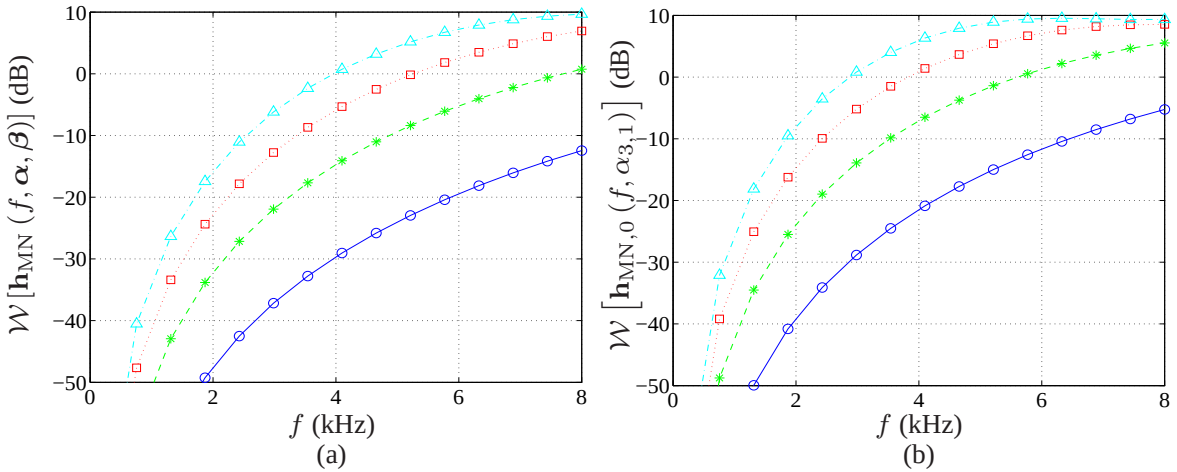

Figure 24: WNG of third-order DSAs with minimum-norm filters as a function of frequency, for different values of M: $M = 4$ (solid line with circles), $M = 6$ (dashed line with asterisks), $M = 8$ (dotted line with squares), and $M = 10$ (dash-dot line with triangles). (a) Third-order DSA with three distinct nulls, $\mathbf{h}_{\mathrm{MN}}(f, \boldsymbol{\alpha}, \boldsymbol{\beta})$, and (b) third-order cardioid, $\mathbf{h}_{\mathrm{MN},0}(f, \alpha_{3,1})$, with $\alpha_{3,1} = -1$.

Table 1: Differential beamformers.

First-Order:	$\mathbf{h}_1(f) = \frac{1}{1 - e^{\jmath 2\pi f \tau_0 \left(1-\alpha_{1,1}\right)}} \begin{bmatrix} 1 \\ -e^{-\jmath 2\pi f \tau_0 \alpha_{1,1}} \end{bmatrix}$
Second-Order:	$\mathbf{h}_2(f) = \mathbf{U}(f)\mathbf{L}(f) \begin{bmatrix} 1 \\ \beta_{2,1} \\ \beta_{2,2} \end{bmatrix}$
	$\mathbf{h}_{2,0}(f) = \frac{1}{\left[1 - e^{\jmath 2\pi f \tau_0 \left(1-\alpha_{2,1}\right)}\right]^2} \begin{bmatrix} 1 \\ -2e^{-\jmath 2\pi f \tau_0 \alpha_{2,1}} \\ e^{-\jmath 4\pi f \tau_0 \alpha_{2,1}} \end{bmatrix}$
Third-Order:	Equation (81)
	$\mathbf{h}_{3,0}(f) = \frac{1}{\left[1 - e^{\jmath 2\pi f \tau_0 \left(1-\alpha_{3,1}\right)}\right]^3} \begin{bmatrix} 1 \\ -3e^{-\jmath 2\pi f \tau_0 \alpha_{3,1}} \\ 3e^{-\jmath 4\pi f \tau_0 \alpha_{2,1}} \\ -e^{-\jmath 6\pi f \tau_0 \alpha_{2,1}} \end{bmatrix}$
Hypercardioid:	$\mathbf{h}_{\mathrm{Hd}}(f) = \frac{\mathbf{\Gamma}_{0,\pi}^{-1}(f)\mathbf{d}\left(f,1\right)}{\mathbf{d}^H\left(f,1\right)\mathbf{\Gamma}_{0,\pi}^{-1}(f)\mathbf{d}\left(f,1\right)}$
Supercardioid:	$\mathbf{h}_{\mathrm{Sd}}(f) = \frac{\mathbf{t}_1(f)}{\mathbf{d}^H\left(f,1\right)\mathbf{t}_1(f)}$
Minimum-Norm:	$\mathbf{h}_{\mathrm{MN}}\left(f,\boldsymbol{\alpha},\boldsymbol{\beta}\right) = \mathbf{D}^H\left(f,\boldsymbol{\alpha}\right)\left[\mathbf{D}\left(f,\boldsymbol{\alpha}\right)\mathbf{D}^H\left(f,\boldsymbol{\alpha}\right)\right]^{-1}\boldsymbol{\beta}$
	$\mathbf{h}_{\mathrm{MN},0}\left(f,\alpha_{N,1}\right) = \mathbf{D}_0^H\left(f,\alpha_{N,1}\right)\left[\mathbf{D}_0\left(f,\alpha_{N,1}\right)\mathbf{D}_0^H\left(f,\alpha_{N,1}\right)\right]^{-1}\mathbf{i}_1$

[1] J. Benesty, J. Chen, and Y. Huang, *Microphone Array Signal Processing*. Berlin, Germany: Springer-Verlag, 2008.

[2] G. W. Elko and J. Meyer, "Microphone arrays," in *Springer Handbook of Speech Processing*, J. Benesty, M. M. Sondhi, and Y. Huang, Eds., Berlin, Germany: Springer-Verlag, 2008, Chapter 50, pp. 1021–1041.

[3] G. W. Elko, "Superdirectional microphone arrays," in *Acoustic Signal Processing for Telecommunication*, S. L. Gay and J. Benesty, Eds. Boston, MA: Kluwer Academic Publishers, 2000, Chapter 10, pp. 181–237.

[4] J. Benesty and J. Chen, *Study and Design of Differential Microphone Arrays*. Berlin, Germany: Springer-Verlag, 2012.

[5] J. Chen, J. Benesty, and C. Pan "On the design and implementation of linear differential microphone arrays," *J. Acoust. Soc. Am.*, vol. 136, pp. 3097–3113, Dec. 2014.

[6] R. N. Marshall and W. R. Harry, "A new microphone providing uniform directivity over an extended frequency range," *J. Acoust. Soc. Am.*, vol. 12, pp. 481–497, 1941.